frontiers | Frontiers in Marine Science

ORIGINAL RESEARCH
published: 18 July 2022
doi: 10.3389/fmars.2022.825359

Numerical Simulation of the Locality of Erosional Damages by Storm Waves in Searching for Measures to Conserve Bonggil Beach, Korea

*Jong Dae Do[1], Jae-Youll Jin[1], Byunggil Lee[1], Weon Mu Jeong[2], Jin Yong Choi[3], Sang Kwon Hyun[4], Kihyun Kim[5] and Yeon S. Chang[2]**

[1]East Sea Environment Research Center, Korea Institute of Ocean Science and Technology, Uljin, South Korea, [2]Maritime Information and Communication Technology (ICT) R&D Center, Korea Institute of Ocean Science and Technology, Busan, South Korea, [3]Marine Disaster Research Center, Korea Institute of Ocean Science and Technology, Busan, South Korea, [4]Sekwang Engineering Consultants Company Limited, Seoul, South Korea, [5]Department of Coastal Management, GeoSystem Research Corporation, Gunpo, South Korea

OPEN ACCESS

Edited by:
Giandomenico Foti,
Mediterranea University of Reggio Calabria, Italy

Reviewed by:
Jianjun Jia,
East China Normal University, China
Effi Helmy Ariffin,
University of Malaysia Terengganu, Malaysia

***Correspondence:**
Yeon S. Chang
yeonschang@kiost.ac.kr

Specialty section:
This article was submitted to Coastal Ocean Processes, a section of the journal Frontiers in Marine Science

Received: 30 November 2021
Accepted: 08 June 2022
Published: 18 July 2022

Citation:
Do JD, Jin J-Y, Lee B, Jeong WM, Choi JY, Hyun SK, Kim K and Chang YS (2022) Numerical Simulation of the Locality of Erosional Damages by Storm Waves in Searching for Measures to Conserve Bonggil Beach, Korea. Front. Mar. Sci. 9:825359. doi: 10.3389/fmars.2022.825359

Coastal erosion caused by extreme storms can reduce the value of beaches. Under the scenario of climate change, the storm intensity may increase and the resulting severe erosion can lead to disastrous damages on the beaches. Therefore, it is crucial to find appropriate measures and adaptation plans to conserve the beach from storm attacks. In this study, numerical models were applied to analyze the dune erosion in Boggil Beach, Korea, occurred by Typhoon Tapah in September 2019. Two models were used as Telemac-2D was run in larger domains for producing forcing conditions. XBeach was then applied to simulate the 2019 dune erosion after validation using observational data from a post-event field experiment performed in 2020. The model results showed reasonable agreement with the observational data except for the overestimation of erosion that was likely caused by characteristic pattern of sediment that was a mixture of sand and gravel and the accuracy of model results decreased due to the existence of gravel. The results also confirmed the locality of erosional damage by which the dune erosion was severest in the southern part of the beach. This locality was caused because the water depth was steeper in this area, which kept the wave energy in this area higher than that in the northern part. The uneven distribution of depth was induced by natural and anthropogenic causes. Three cases of model tests were performed to determine an appropriate measure to preserve the beach from future storm attacks – two were to place a submerged breakwater (SB), and one to place a submerged groin(SG). Although the SBs could directly protect the shore from erosion in the lee of the SBs, they could cause additional erosions at unexpected seabed areas. Although the SG was not the best in protecting the beach from the dune erosion, it could minimize the side effect. This measure was also environmentally friendly by keeping the sediments within the coastal cell around the SG so that the beach maintenance could be feasible through replenishment. In addition, the SG could also save the initial cost by reducing its size, and would be more effective, if the recovery process considered, because the SBs would disturb the onshore sediment motions under milder wave conditions. The results of this

study can be applied for decision-making to establish future adaptation plans from storm impacts in Bonggil Beach.

Keywords: coastal erosion, shoreline change, storm waves, xbeach surfbeat, telemac-2D

1 INTRODUCTION

Coastal erosion has become a serious problem in many coastal areas in the world. The reason for the increasing threat on the coasts by erosion may be found from the natural factors such as climate change (Zhang et al., 2004; Masselink and Russell, 2013; Mentaschi et al., 2018) and from the anthropogenic factors such as coastal structures (Syvitski et al., 2005; van Rijn, 2011; Anthony et al., 2015). For example, episodic events of severe coastal erosion would increase when the intensity of storms increases due to the warming of sea surface (Bender et al., 2010; Knutson et al., 2010), and when the equilibrium within a coastal cell could be broken by construction of coastal structures (Do et al., 2021a). Because climate change is an ongoing process and will continue unless robust actions are taken globally, and also because various engineering structures will continue to be built as the coastal communities grow worldwide, the problem of erosion may remain as a significant issue not only at present but also in the future for probably a considerable time. Therefore, it is necessary to develop measures and plans to mitigate the damage by coastal erosion based on proper risk assessment. These assessments and measures should be carefully set up because the impact by coastal erosion is site-specific due to characteristic conditions in a coastal area and sometimes shows locality even within the same area due to the loss of equilibrium by various factors (Oh et al., 2021). Accurate analysis of sediment transport patterns is, therefore, a prerequisite to developing such measures for the site.

The characteristic pattern of sediment transport can be understood by analyzing the short-term and/or long-term sediment budget, the balance between the added and removed sediments within the coastal cell. However, accurate prediction of coastal sediment transport is difficult because the waves carry the sediment both onshore and offshore directions under different conditions. In addition, wave-induced currents and resulting nearshore circulations can lead to complex pattern of sediment transport within the coastal cell, which adds difficulties in understanding their motions. Therefore, the study of coastal sediment transport requires correct information on the hydrodynamic and geographic conditions in the nearshore areas. In addition, factors such as sediment inputs by streams, littoral drift, and outputs in the offshore and longshore directions would be important to understand the balance of the sediment budget within the coastal cell.

In general, the sediments in the beachface move offshore under energetic wave conditions (Russell, 1993), resulting in the shoreline retreat in a short time scale in days or even in hours (Harter and Figlus, 2017; Davidson-Arnott et al., 2019). The eroded shorelines are recovered in months, as a natural process, under mild wave conditions following the storms due to slow but steady onshore sediment motions caused by wave nonlinearity (Hsu and Hanes, 2004), which results in the balance of the shoreline positions without retreat or advancement in the long run. However, under specific conditions such as extraordinary storm waves, the damage on the shore could be too severe so that the recovery process may take a long time of years or even decades (Forbes et al., 2004) because the high wave power under these storms could carry the sediments to the areas where the waves and currents could not affect the sediment motion under normal wave conditions (Do et al., 2019). Sometimes, the damage could hardly be recovered when the coastal structures built to protect the shore were broken (Do et al., 2021a). In order to prevent unexpected damage and to find proper protection plans for beaches of economic and cultural values, therefore, it is important to accurately predict the processes under extreme conditions, considering that the intensity and frequency of major storms may increase in the coming years due to climae change (Bender et al., 2010; Knutson et al., 2010).

In the present study, we observed a severe coastal erosion in Bonggil Beach of the Republic of Korea when Typhoon Tapah attacked the site in late September 2019, which was classified as Categoty 1 tropical cyclone (1-minute maximum sustained wind speed for Category 1 ranges 33-42 m/s). Although the typhoon was not a major storm, it led to huge damages in the beaches located on the east coast of Korea due to the geographical proximity of its path. Specifically, the pattern of damage was distinguished in Bonggil Beach because the erosion showed strong locality as the damage was focused in the southern part of the beach that is separated from the northern part by a nearshore rocky island. In contrast, the typhoon left less severe damage in the northern part that is connected to a stream. In addition to Typhoon Tapah, additional tropical cyclone, Typhoon Mitag, attacked the site consecutively in early October. Typhoon Mitag was classified as Category 2, whose wind speed ranges 43-49 m/s. Considering the unprecedented damage made on the beachface, this study was initiated to analyze and understand the nearshore and beach processes that occurred in the site during the storms, specifically to support the decision-making by the local government to establish appropriate plans to protect and preserve the beach from future threats by similar or even worse storm waves.

For this, we performed field experiments to measure topography and hydrodynamic data and searched for historical records on the site. We also used XBeach model (Roelvink et al., 2009) to simulate the processes during the storm events. Commonly employed area models such as Telemac-2D (Galland et al., 1991) and Delft3D (Roelvink and Van Banning, 1995) have been used to calculate sediment transport, based on the hydrodynamic conditions calculated by the wave and flow modules. However, they are designed to calculate the changes

in seabed elevation, which can be applied to indirectly estimate the shoreline changes. In contrast, the surfbeat mode of XBeach can simulate the morphological changes in the beachface outside the water under extreme wave conditions by resolving the long wave motions with an additional module for avalanching – the slumping of sand from dune face to foreshore under high wave conditions.

In addition, the impacts of sediments that have different sizes at one location can be considered by XBeach in simulating the sediment transport and the resulting morphological changes, using multiple sediment classes with different fractions of each size. One of the characteristic pattern of the sediment in Bonggil Beach was that it was a mixture of sand and gravel. In particular, the spatial distribution of the sand and gavel fractions showed strong loaclity withing the beach area, which required special setting in the input of sediment conditions to reduce modeling error. There were previous studies using XBeach that used multiple sediment classes, especially for the simulation in the gavel (Jamal et al., 2014; McCall et al., 2015) or sand and gravel mixture coasts (Bergillos et al., 2016). However, most of them were 1-dimensional approaches to focus the cross-shore directional sediment transport based on XBeach-G (McCall et al., 2015; Phillips et al., 2020). Recently, 2-dimensinal version of XBeach was used with three sediment classes and their different spatial distributions based on sediment samplings at multiple locations (Gurov and Fomin, 2021). However, their sediments ranged within sand and the impacts by larger sediment grains such as gavel was not examined.

In this study, we investigated the course of the erosional process in the beachface of Bonggil Beach using 2-dimensional Xbeach surfbeat. The model was elaborately setup with the additional application of an area model, Telemac-2D, to provide the forcing conditions by the storm waves to the XBeach. In particular, the sediments were sampled at 72 locations in the beachface and in the water, and the sediment data were classified into two groups of sand and gravel so that the impact of sediment condition could be carefully considered with different sand-gravel fractions at each grid point. The modeling was then focused to generate the exceptional erosion in Bonggil Beach, and thus to analyze the conditions that caused the unusual erosion event. The model was validated based on observational data obtained from field experiments. Once the analysis of the episodic erosion events was completed, additional simulations were performed to search for appropriate measures to mitigate future damages from the attacks of similar or even greater storm events in the study site.

The final goal of this study was then to develop an effective and economic engineering measure to reduce the potential damages by future storm waves, for supporting decision-making to establish conservation plans for Bonggil Beach. Usually, conservation plans for beaches that are vulnarable to storm attacks are established based on the severity of the storms. For exmple, Klima et al. (2012) calculated surge height and wind speed as functions of return period in the areas of Miami-Dade County, United States, and estimated costs and econimic losses using damage models to set up damage reduction protfolios. The present study was not aimed to provide an adaptation plan from storm attacks considering the intensity of future typhoons. Instead, the study was designed to understand the characteristic patern of storm damage spedified in the study site, then to provide possible measures to prevent the similar damage from future storm attacks. Therefore, its study goal was to develop a site-specific engineering measure in Bongil Beach, and the outcome could be confined in this study area, instead of being widely applied for storm adaptation.

The paper is organized as follows. The information of the study site and the damages made by Typhoon Tapah are described in Sections 2.1 and 2.2, respectively. The field experiments performed after the storm event are introduced in Section 3.1. The setup of XBeach and Telemac-2D models in the site is described in Sections 3.2 and 3.3. Validation of the models is described in Section 4.1, and the model results are analyzed in Sections 4.2 and 4.3. The discussions on model outcomes and the suggestions of measures to protect the beach for future storm attacks are provided in Section 5, and the conclusion of the study is in Section 6.

2 BACKGROUND

2.1 Study Site

Bonggil Beach is located on the southeast coast of the Korean Peninsula (**Figure 1A**). It is a 1.8 km long beach whose shoreline is straight in the NNW-SSE direction, facing NEE. **Figure 1B** shows a map of Bonggil Beach, captured from Google Earth on July 4, 2019. The beach consists of a small coastal cell because its northern end is blocked by a set of breakwaters (P1) around a fishing port, and small-sized rocky islands and underwater rocks (P4) are located at the southern end, making the water depth shallower, which disturbs alongshore sediment movement toward further south. In addition, the sediments that are lost from the southern end can hardly be recovered because the shoreline is bent to SSW due to an artificial bank (P5) that was constructed along the shore using tetrapod in order to protect Wolseong Nuclear Power Plant (WNPP). In between the two ends, there is a source of sediment input to the beach through Daejong Stream (P2). One of the most significant features of Bonggil Beach is the rocky island located in the middle of the beach (P3). The island has a diameter of ~50 m and is located ~150 m away from the shore, where the water depth is ~5 m, which disturbs wave propagation, causing a salient in the coast behind the island. This island is culturally important because, according to a legend, this island has been known to be the tomb of a heroic king in Korean history. The island has a name, 'MunMu-daewang-neung' (meaning 'Tomb of Great King MunMu'). For this reason, Bonggil Beach has been one of the most famous beaches in this region where many tourists visit.

The wind and wave condition is moderate in this region as shown with the wind and wave roses in **Figures 2C**, **D**. The wind usually blows from land (WNW) and the wind speed are mostly no greater than 8 m/s. The annual mean significant wave height (H_s) is 0.8 m with the peak wave period of 6.5 s. The most common wave propagation direction is NE and ENE (from the left in **Figure 1B**) as observed from the wave measurement by an AWAC (Acoustic Wave and Current Profiler) located 6.5 km south

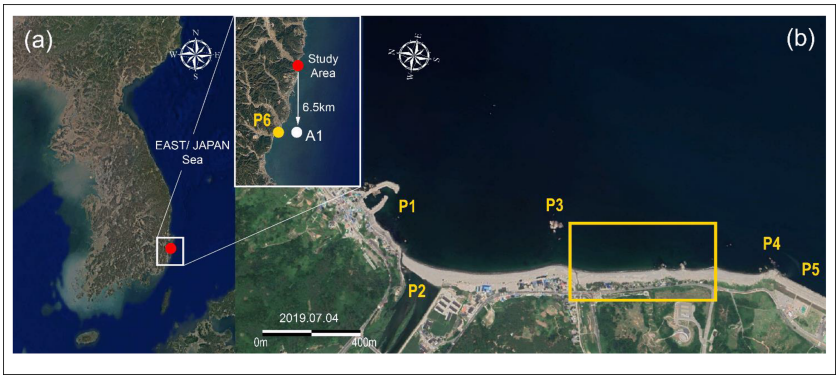

FIGURE 1 | (A) Location of Bonggil Beach in the Korean Peninsula (red dot). In the magnified view of the study area, the location of A1 is marked (white dot) where the wave data were measured during Exp. 1 and 2. **(B)** Google map of Bonggil Beach on July 14, 2019. P1 – P5 mark the locations of the breakwater in the northern end of the beach (P1), the mouth of Daejong Stream (P2), island 'Tomb of Great King MunMu' (P3), rocky islands and underwater rocks in the southern end of the beach (P4) and artificial bank to protect WNPP (P5). The yellow rectangle marks the southern part of the beach, where the damage by erosion was severe. In the panel located in the upper-left corner of **Figure 1B**, the locations of A1 where the wave data in **Figure 4** were measured, and P6 where the severe road destruction in **Figure 3A** occurred are marked.

of Bonggil Beach at a water depth of ~32 m (A1 in **Figure 1A**). In addition to NE, waves are also commonly approaching from SE (from the right in **Figure 1B**). The sediment in Bonggil Beach is characterized as a mixture of sand and pebbles, with their size widely varying from 0.44 mm to 3.22 mm. **Figure 2A** shows a photograph of the beachface in Bonggil Beach on October 24, 2019. The surface of the foreshore (from swash zone to beach berm) is mainly covered by pebbles, whereas the mixture of sand and pebbles are common in the swash zone. Because the sediment in the study site shows characteristic pattern as two types of sediments with clearly different sizes, the measurement was carefully conducted as sediment samples were captured at 72 locations in the beach and in the water (**Figure 2B**). Among them, 30 locations were selected in the beachface (outside water) and 42 locations were inside the water where the sediments were sampled by grab sampler. The details of sediment sampling and the input of sediment data into the numerical model will be described in Section 3.1 and 3.3.

Traditionally, Bonggil Beach has been understood as a depositional beach whose shoreline is gradually advancing due to the excessive input of sediments through Daejong Stream (P2). As shown in **Figure 1B**, the majority part of the stream mouth is blocked by the sediments in the beachface, which has been commonly observed under normal weather conditions. In the rainy season, however, the river mouth is open due to the increased amount of downstream flows that provide sediment to the beach, as shown in **Figure 2C**. It was also reported by the local government that the shoreline positions in the mouth of Daejong Stream are closely related to the precipitation, which indicates that the sediments are carried downstream to the river mouth in heavy rainfalls and transported to the beach, providing a depositional condition in Bonggil Beach.

2.2 Storm Events

On September 22, 2019, Typhoon Tapah passed through the Korean Strait. Tapah was a Category 1 typhoon but caused severe damages, specifically in the southeast coasts of Korea, where the study site is located, due to the proximity of its path. For example, a coastal road in the nearby area (Kyeongju-si Yangnam-myeon) located ~7.0 km south of Bonggil Beach, was destroyed by the storm waves of Typhoon Tapah, as shown in **Figure 3A**. Damage by Tapah was severe in Bonggil Beach, especially in the southern part (yellow rectangle in **Figure 1B**). The two pictures in **Figures 3B**, **C** compare the beach status before (May 30, 2019) and after (October 9, 2019) the attack of Typhoon Tapah. Before Tapah, a dune was located in the backshore of the beach, and it was covered by grasses. Behind the dune, pine trees were planted protecting the temporary building. After Tapah, however, the dune was severely destroyed, and a steep berm was formed instead. It is also observed that a pine tree was rooted out and laid down in front of the berm. The damage found in **Figure 3C** was too severe, and the natural recovery of the beach seems difficult or may take a long time. After Typhoon Tapah, another tropical cyclone, Typhoon Mitag, attacked the Korean Peninsula on October 3, 2029. Although Mitag was a Category 2 typhoon (max. wind speed 40 m/s), damages made in the study site and in the vicinity were much smaller because its strength became weaker once it landed on the southwestern coast and passed through the peninsula. The wave data measured during Tapah and Mitag are provided in Section 3.1, and the paths of the two typhoons are marked in **Figure 8A**.

3 MATERIAL AND METHODS

3. 1 Field Observations

There are sets of observational data available near the study site for comparisons before and after the event of Typhoon Tapah and Mitag. As shown in **Figure 4**, the AWAC in A1 (**Figure 1B**) measured the wave data during Tapah and Mitag at a water depth of ~32 m (**Figure 4**). The maximum significant wave height (H_s) reached ~7 m on September 22, 2019 when Tapah attacked the site. However, it was much reduced (< 4 m) on October 3, 2019

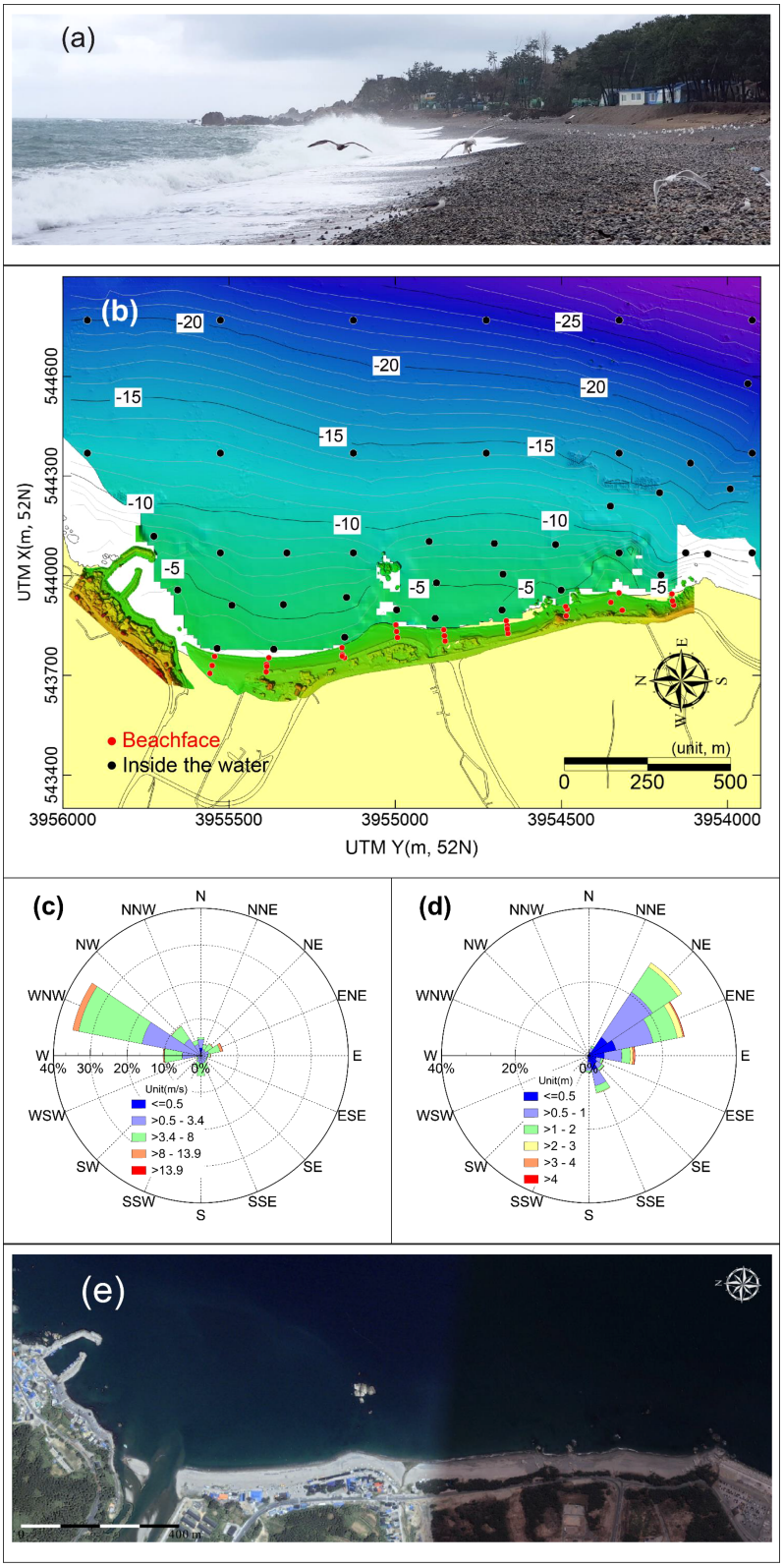

FIGURE 2 | (A) Photograph of the beachface in Bonggil Beach on October 24, 2019, showing the sediment mixture of sand and pebbles. **(B)** Map of the sediment sampling locations, **(C)** wind rose measured at Gampo Port located ~8 km north of the study area, **(D)** wave rose measured at A1 (**Figure 7**) in the study area, **(E)** Google Earth image on July 17, 2011, which shows that the stream mouth was open.

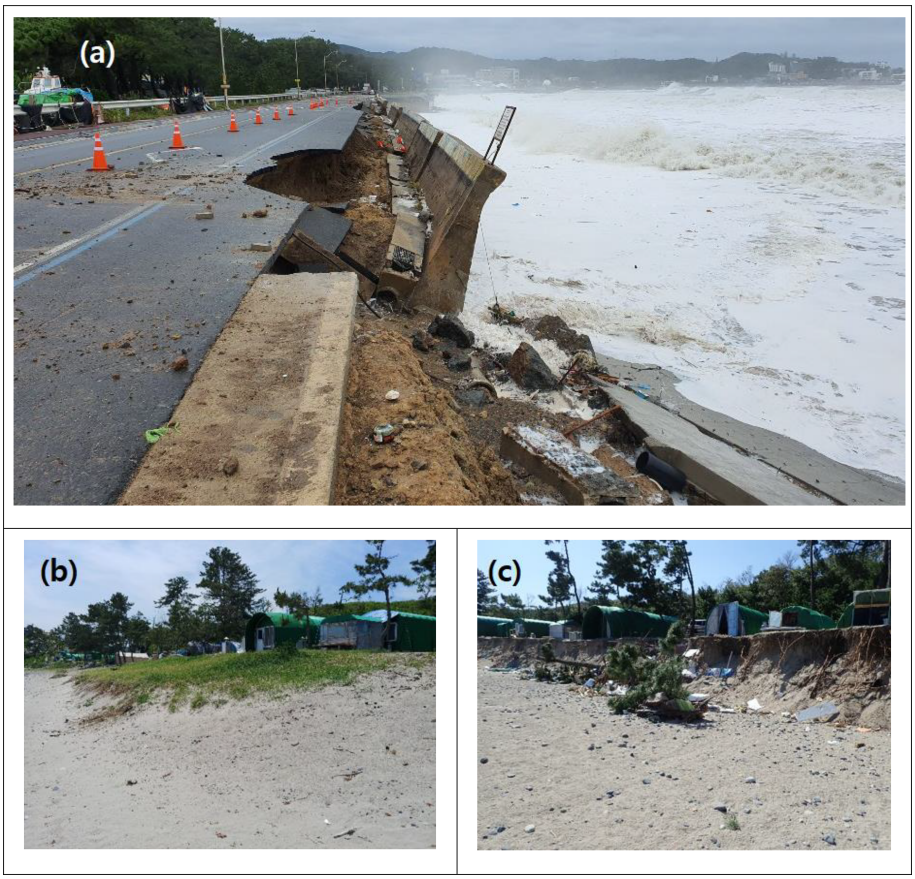

FIGURE 3 | (A) Picture of coastal road destroyed by the attack of Typhoon Tapah, captured from Newsis newspaper (https://newsis.com/view/?id=NISX20190923_0000777231&cID=10899&pID=10800). The road was located ~7.0 km south of Bonggil Beach (P6 in **Figure 1B**) with address of Haebyeongongwon-gil, Yangnam-myeon, Gyeongju-si, Gyeongsangbuk-do, Republic of Korea 38220. **(B)** Picture of the southern part of Bonggil Beach (yellow rectangle in **Figure 1B**) before the attack of Typhoon Tapah (May 30, 2019), and **(C)** picture of the same part of the beach, but after Typhoon Tapah (October 9, 2019).

when Mitag attacked. Because the pictures in **Figures 3A** and **C** were taken after Mitag, it was unclear that the damages in this area were only done by Tapah or by the two consecutive tropical cyclones. However, considering the significant difference in the measured wave height and the witnesses from the dwellers in this area, the damages were presumed to be mostly caused by Tapah. The period of the two storm attacks in **Figure 4** is set as Exp. 1 (September 15 – October 21, 2019), in which the severe coastal erosion in the study site occurred. In addition to the wave measurements, geography data were also available on the site as the profiles, the elevation of beachface, were measured along the perpendicular lines to the coast from October 2019 to October

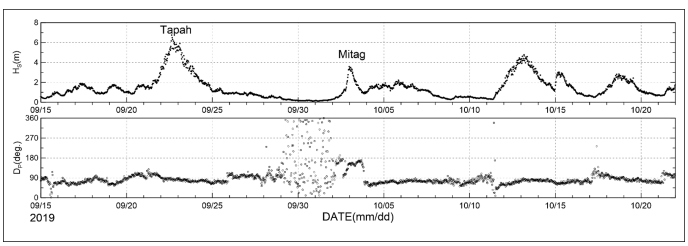

FIGURE 4 | Time series of significant wave height (H_s) and peak wave direction (D_p) from September 15 to October 21, 2019, covering the times of Typhoons Tapah and Mitag, measured by the AWAC at A1 (**Figure 1B**), located 6.5 km south of Bonggil Beach at a water depth of ~32 m. The period of 37 days in **Figure 4** is set as Exp. 1 as it included the period of the erosional event in Bonggil Beach, shown in **Figure 3**. D_p is in degree measured in the clockwise direction from the north (i.e. 45 ° =NE; 90 ° =E; and 135 ° =SE).

2020. **Figure 5A** marks the locations of six profiles (Line 1 – Line 6) on a map measured by a drone on October 20, 2020. The drone was DJI Phantom 4 RTK with takeoff weight of 1.4 kg and diagonal distance of 35 cm, and the three-dimensional meshes were calculated through GCP calibration. The hover accuracy range was ±0.1 m in the vertical and ±0.1 m in the horizontal. The camera resolution was 20 MP, and the GCP RMSE was 4.9 cm and 2.1 cm in the horizontal and 2.5 cm in the vertical. In **Figure 5B**, the beachface elevation data that was measured four times (2019/05/30, 2019/10/09, 2020/09/10, 2020/10/20) before and after the period of Typhoon Tapah and Mitag are compared along with the nine profile lines. The data show high variability with a maximum range of ~3 m, indicating the elevation fluctuated actively in time. However, it does not confirm the specific pattern of erosion or accretion in the site except for Line 7 that is located in the southern part of the beach. Along Line 5, the shoreline was retreated for ~7 m since November 2018 and could not be recovered until October 2020. The location of Line 5 corresponds to the location of severe erosion shown in **Figures 3B**, **C**. Thus the shoreline retreat along Line 5 was likely caused by the storm waves during the attacks of Typhoon Tapah and Mitag.

Because the profile data and the wave measurements from the site were not sufficient to validate the model results, an additional (post-event) field experiment (Exp. 2) was performed from September 15 – October 21, 2020. Exp. 2 was designed to measure geographic and hydrodynamic data such as waves, currents, and suspended sediment concentration using instrument frames that mounted acoustic sensors (Do et al., 2019). During the period of Exp. 2, storm waves also affiliated the southeast coast of, which provided comparable conditions with the times in 2019 when the typhoon Tapah attacked the site. It is noted that the intensity of the storms during Exp. 2 was weaker than that of Tapah in Exp. 1, and the damage by coastal erosion in 2020 was observed to be weaker than that in 2019. The wave condition during Exp. 2 is shown in **Figure 6** when comparing with the model results for validation, and it is not plotted in this section to avoid repetition.

The bathymetry was measured using single-beam (< 3 m) and multi-beam (> 3 m) echosounders, and **Figure 7A** shows the bathymetry data measured on October 21, 2020. The hydrodynamic data were measured during the period of Exp. 2 as well. In **Figure 7A**, the location of the instrument frame (B1) is marked, and **Figure 7B** shows the picture of the frame at B1. The instruments mounted on each frame and their measured data are listed in **Table 1**. The data measured in Exp. 2 are analyzed in Section 4.1. It is noted that, from the bathymetry data in **Figure 7A**, the water depth was deeper in the southern part of the beach (the area where B1 is located). The difference in the water depth can be observed by comparing the distance between the contour lines of -5 m and -10 m. The distance was shorter in the southern part, which indicates that the slope of seabed was steeper in this area. Therefore, the water depth was deeper in the nearshore of the southern part when it was compared at the same distance from the shore.

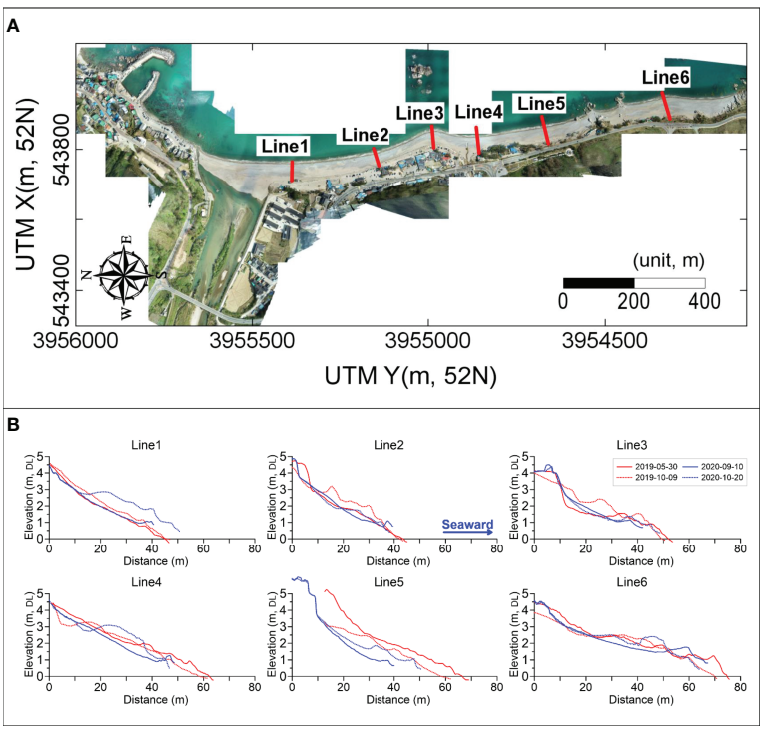

FIGURE 5 | (A) Locations of the six profiles marked on a map measured by a drone survey on October 20, 2015. The profiles were measured four times before and after Typhoon Tapah and Mitag from May 2019 to October 2020. **(B)** Comparisons of profile measurement along the nine lines for the four times on 2019/05/30 (red solid), 2019/10/09 (red dashed), 2020/09/10 (blue solid), 2020/10/20 (blue dashed).

TABLE 1 | List of the instruments mounted on the frame at B1.

Location	Depth	Instruments	Manufacturer	Sampling Interval	Burst Interval	Sampling Frequency	Transducer Frequency	Measurement
129° 29' 10.80" E	~5 m	VECTOR	Nortek AS	600 sec	3600 sec	8 Hz	6 MHZ	Wave parameters and near-bed flow velocities (0.4 m above seabed)
35° 44' 08.41" N		WBL	RBR Ltd.	128 sec	1800 sec	4 Hz	0.2 MHz	Seabed elevation change(0.9 m above seabed)

As described in Section 2.1, the sediment in the study site was a mixture of sand and gravel. In order to carefully analyze the sediment characteristics in this site, therefore, the sediment samples were captured at 72 locations in the beach as well as in the water (the sediments in the water were sampled by grab sampler). D50, D10 and D90 were obtained at each sampling locations. In addition, the proportions of sand, gravel, silt and clay have been obtained at each location (for example, the proportion of sand, gravel, silt and clay at location B20 [one location in the beachface] was 86.75%, 13.25%, 0.00% and 0.00%, respectively, so that the sum of each proportion gave 100% at each location). Based on these sediment proportion data, the sediment facies at each location has been classified into two groups. The two groups are *S* (Sand dominant) and *G* (Gravel dominant). For example, the sediment facies at B20 was classified as *S*. Once the sediment samples at each location are classified, two sediment sizes, D50, were obtained representing the two groups (i.e. D50 = 0.44 mm for group S, whereas D50 = 2.34 mm for Group G). The reason to classify the sediment size into the two groups and obtain the two D50s was to input the two D50s in the model, considering their proportions, which will be described in Section 3.3.

3.2 Numerical Models

In this study, two different models were used to simulate the storm impacts. These models are briefly described in this section as they were introduced in detail by the developers. First, the Telemac -2D (Galland et al., 1991) was employed to generate the wave fields using the wind fields obtained from the Japanese Meteorological Agency (JMA) during the experimental periods. Its results were then applied to produce the time-varying boundary conditions for the XBeach surfbeat (Roelvink et al., 2009) model that was to simulate the seabed topography and shoreline changes by the storm attacks. Telemac-2D is 2DH model package with modules for flows, waves, and sediment transport. This model is characterized by the unstructured mesh system in the horizontal, which has been effectively applied in the coastal regions with complicated topography (Do et al., 2020). Because Telemac-2D only simulated the morphology changes on the seabed but was not to directly calculate the morphological changes along the shore and outside the water, its application for the erosion process in the beachface was limited.

The flow module of Telemac-2D is based on the shallow water equation that solves the depth-averaged momentum equations

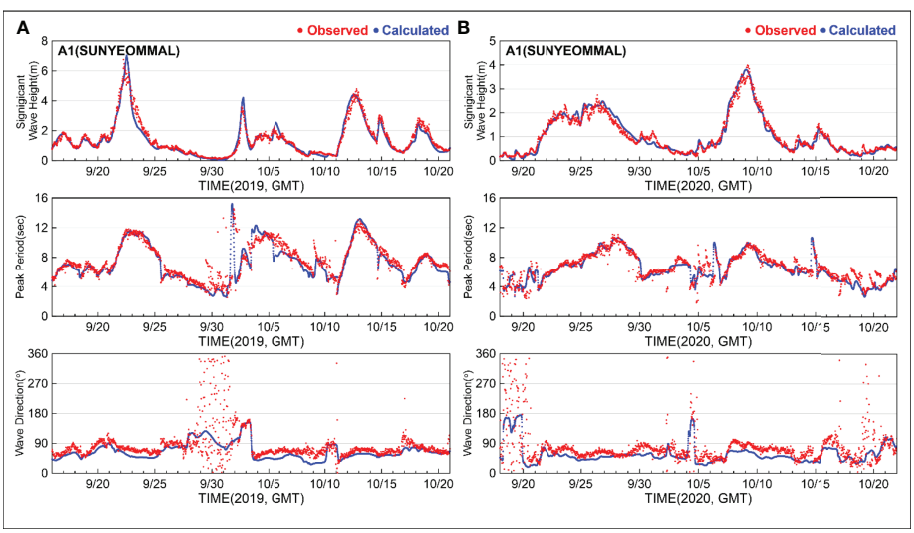

FIGURE 6 | (A) Comparison of significant wave heights (H_s, top panels), peak wave period (T_p, middle), and wave propagation direction (D_p, bottom), between the measured (red dots) and Telemac-2D & Tomawac model (solid blue lines) data at A1 for Exp. 1 (September 15 – October 21, 2019; left panels), and **(B)** for Exp. 2 (September 15 – October 21, 2020; right panels).

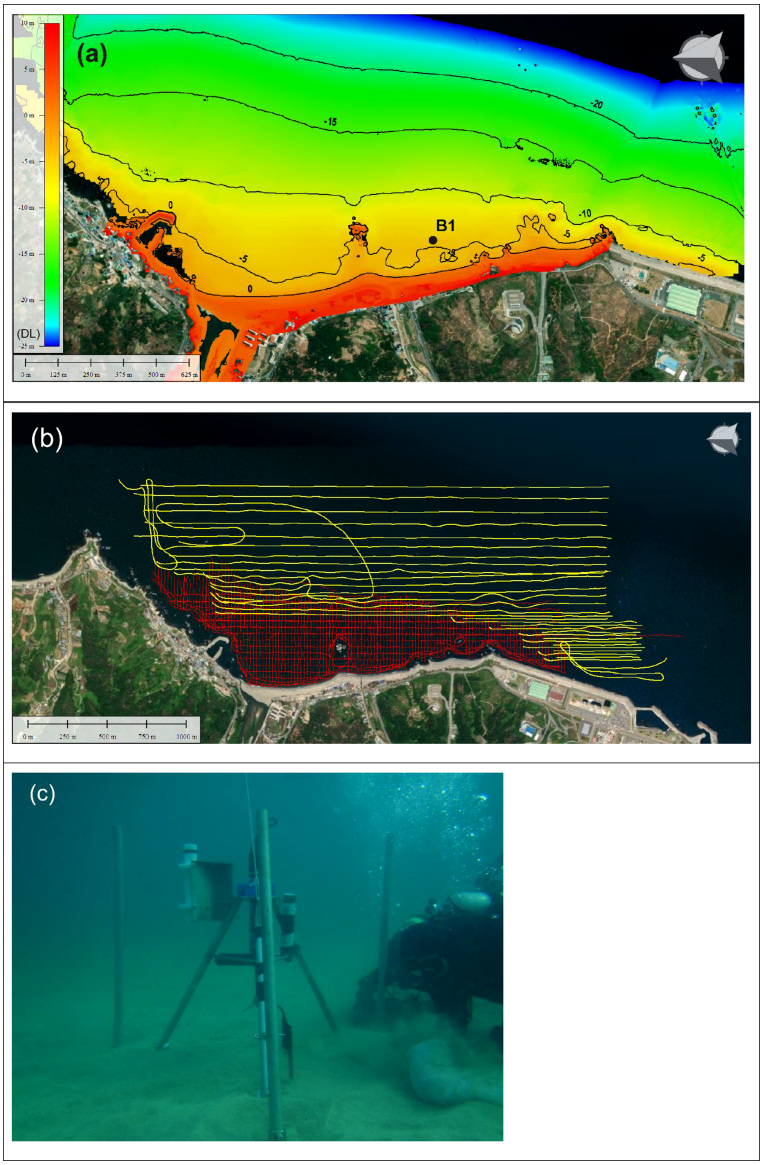

FIGURE 7 | (A) Map of water depths in Bonggil Beach measured by single-beam and multibeam echosounders on October 21, 2020. The single-beam measured data at shallow areas (< 3 m) where the ship with multibeam could not cover. B1 was the location where the instrument frame (**Figure 7B** and **Table 1**) was moored, **(B)** the map of track lines of the bathymetry measurements by single-beam (red) and multi-beam (yellow) echosounders, and **(C)** picture of the underwater-mounted instrument frame.

and continuity equation (Asaro and Paris, 2000; Hervouet, 2000; Robins and Davies, 2011) as:

$$\frac{\partial h}{\partial t} + u\bullet\vec{\nabla}(h) + h\bullet div(\vec{u}) = S_h$$

$$\frac{\partial u}{\partial t} + \vec{u}\bullet\vec{\nabla}(u) = -g\frac{\partial \eta}{\partial x} + S_x + \frac{1}{h}div\left(h\nu_t\vec{\nabla}u\right)$$

$$\frac{\partial v}{\partial t} + \vec{v}\bullet\vec{\nabla}(v) = -g\frac{\partial \eta}{\partial y} + S_y + \frac{1}{h}div\left(h\nu_t\vec{\nabla}v\right)$$

where h is water depth, ν_t is the diffusion coefficient, η is the free surface elevation, S_h S_x and S_y are the source/sink. In the Telemac-2D of this study, the forcing was initially given by the wind fields that were used to generate the wave fields. For the wind fields of the selected storm conditions, JMA was used. The wave fields were generated using the wave module, named 'Tomawac,' which is internally coupled into the Telemac-2D system to generate the wave-induced currents. Tomawac

solves the spectral action balance equation to compute the wave properties such as wave height, period, and wave propagation direction from the wave spectra. Tomawac can also consider the effect of wave diffraction (Holthuijsen et al., 2003) based on the mild slope equation (Berkhoff, 1973). The formulation of the wave action equation is described with the XBeach surfbeat model as it also solves the spectral action balance equation for wave propagation. Once the wave and flow fields are obtained, the sediment transport field can be calculated by solving bedload and suspended load formulas, which then be used to simulate the seabed elevation changes using the morphology module. As already mentioned, the calculation of morphology change is only allowed for the grids inside the water, and the morphological changes outside water are not considered by Telemac-2D. For this reason, Telemac-2D may not be a proper tool for direct evaluation of beachface erosion in the present study, thus used to provide the forcing conditions for the XBeach model in the present study.

The XBeach surfbeat model was able to estimate the rapid changes in the shoreline due to the attacks of storm waves. It is because the model has an additional module, the avalanching module that calculates sand slumping from dune face to foreshore. Thus can be applied to estimate the shoreline evolution. XBeach surfbeat is characterized to resolve the long wave (infragravity) motions, considering that the impacts of long waves are dominant for the shoreline evolution, whereas the shortwaves are often dissipated by breaking and friction when arriving at the shore. Therefore, the surfbeat mode of XBeach does not solve the individual short waves. Instead, it describes the short wave propagation by solving the wave action equation, similar to Telemac-2D, as:

$$\frac{\partial A}{\partial t}+\frac{\partial C_x A}{\partial x}+\frac{\partial C_y A}{\partial y}+\frac{\partial C_\theta A}{\partial \theta}=-\frac{D_w}{\sigma}$$

where $A(x,y,t,\theta)=\frac{S_w(x,y,t,\theta)}{\sigma(x,y,t)}$ is the wave action, θ is the angle of wave incidence, $S_w(x,y,t,\theta)$ is wave energy density, D_w is wave energy dissipation, σ is wave frequency, C_x C_y nd C_θ are wave action propagation speed in the x y and θ direction respectively. The root-mean-square wave height is then calculated from the wave energy spectra as $H_{rms}=\sqrt{8E_w/\rho g}$ where. E_w. is the short wave energy. Once Eqn. (4) is solved, the forcing that generates the long waves is obtained from the radiation stress, which is based on the wave energy variation as:

$$F_x=-\left[\frac{\partial S_{xx}}{\partial x}+\frac{\partial S_{xy}}{\partial y}\right],F_y=-\left[\frac{\partial S_{yy}}{\partial y}+\frac{\partial S_{yx}}{\partial x}\right]$$

where S_{xx} S_{yy} S_{xy} and S_{yx} are the radiation stresses and F_x and F_y are the forcing in the x and y directions, respectively. In XBeach surfbeat, the x axis is located parallel to the coastline, and y -axis is set perpendicular to the shore. The forces in Eqn. (5) are used to generate the long waves *via* the shallow water equation as:

$$\frac{\partial u^L}{\partial t}+u^L\frac{\partial u^L}{\partial x}+v^L\frac{\partial u^L}{\partial y}-fv^L-\nu_h\left(\frac{\partial^2 u^L}{\partial^2 x}+\frac{\partial^2 u^L}{\partial^2 y}\right)=-\frac{\tau_{sx}}{\rho h}-\frac{\tilde{}_{bx}}{\rho h}-g\frac{\partial \eta}{\partial x}+\frac{F_x}{\rho h}$$

$$\frac{\partial v^L}{\partial t}+u^L\frac{\partial v^L}{\partial x}+v^L\frac{\partial v^L}{\partial y}+fu^L-\nu_h\left(\frac{\partial^2 v^L}{\partial^2 x}+\frac{\partial^2 v^L}{\partial^2 y}\right)=-\frac{\tau_{sy}}{\rho h}-\frac{\tilde{}_{by}}{\rho h}-g\frac{\partial \eta}{\partial x}+\frac{F_y}{\rho h}$$

$$\frac{\partial \eta}{\partial t}+\frac{\partial hu^L}{\partial x}+\frac{\partial hv^L}{\partial y}=0$$

where u^L is the Lagrangian velocity which is defined as a particle's distance that travels in one single period of the long wave divided by the corresponding wave period (Wong, 2016). τ_{sx} is wind stress, τ_{bx} is bottom stress, F_x is the forcing in Eqn. (5), h is water depth, ρ is water density, g is gravitation, ν_h is viscosity, f is Coriolis coefficient and η is the water surface elevation of the long waves. The sediment module of XBeach surfbeat solves an advection-diffusion equation as:

$$\frac{\partial hC}{\partial t}+\frac{\partial hCu^E}{\partial x}+\frac{\partial hCv^E}{\partial y}+\frac{\partial}{\partial x}\left[D_x h\frac{\partial C}{\partial x}\right]+\frac{\partial}{\partial y}\left[D_y h\frac{\partial C}{\partial y}\right]=\frac{hC_{eq}-hC}{T_s}$$

where C is volume concentration of sediment, C_{eq} is equilibrium concentration, D_x is sediment diffusivity, T_s is the time of adaptation of entrained sediments. Morphological change in the seabed can be calculated as:

$$\left|\frac{\partial z_b}{\partial t}\right|=\frac{f_{mor}}{(1-P)}\left[\frac{\partial q_x}{\partial x}+\frac{\partial q_y}{\partial y}\right]=0$$

where z_b is seabed level, P is porosity, q_x are sediment flux, f_{mor} is morphology change factor. In the avalanching module, the dune face is set to be slumped when the bed slope exceeds a critical value within one-time step as:

$$\left|\frac{\partial z_b}{\partial x}\right|>m_{cr}$$

where m_{cr} is the critical value. If the condition is satisfied, the dune bed level can be calculated as:

$$\triangle z_b=\left(\left|\frac{\partial z_b}{\partial x}\right|-m_{cr}\right)\triangle x$$

which is used to evaluate the shoreline evolution.

3.3 Model Setup

The Telemac-2D and XBeach surfbeat models were employed for different purposes, as explained in the previous section. The goal of Telemac-2D was to provide the realistic forcing conditions for the XBeach surfbeat runs, and it was run for two large domains, D1 and D2. **Figure 8A** shows the computational domain and unstructured grid system of D1, the largest domain that covered the seas around the Korean Peninsula and parts of the East China Sea and the Northwestern Pacific Ocean. The purpose of D1 runs of Telemac-2D was to provide the forcing conditions for the smaller domain, D2 shown in **Figure 8B**. Telemac-2D in D1 was run to simulate the tide and wave fields so as to compute the tidal elevation, current, wave height, period, and direction along the boundaries of D2.

The unstructured grid system in D1 used 336,264 nodes and 626,069 elements. The tides were composed of the 16 constituents, including M2 and S2. To generate the waves, JMA wind fields were used over the domain with △x and △y of 0.0625 ° and 0.05 °, respectively. In addition to the wind, the air pressure field was applied to increase the model accuracy, specifically during the time of storms. For the air pressure, the data from National Center for Environmental Prediction (NCEP) were applied over the domain with △x and △y f 0.25 °. The JMA and NCEP data were input in the simulation every 3 hours. The model time step, △t was set to 30 s for the tide simulation and 60 s for the wave simulation. In D1, the Telemac-2D model was run for two experimental periods, Exp. 1 and Exp. 2. First, the model was validated based on the observational data available from Exp. 2 as it was run for 37 days September 15 to October 21, 2020. Once the model was validated using the measured data, the model was run from September 15 to October 21, 2019, which was the main run corresponding to Exp. 1 to investigate the impacts of Typhoon Tapah and Mitag on the beach.

Once the model was run over D1, Telemac-2D with Tomawac was run over domain, D2, using the results from the D1 run as

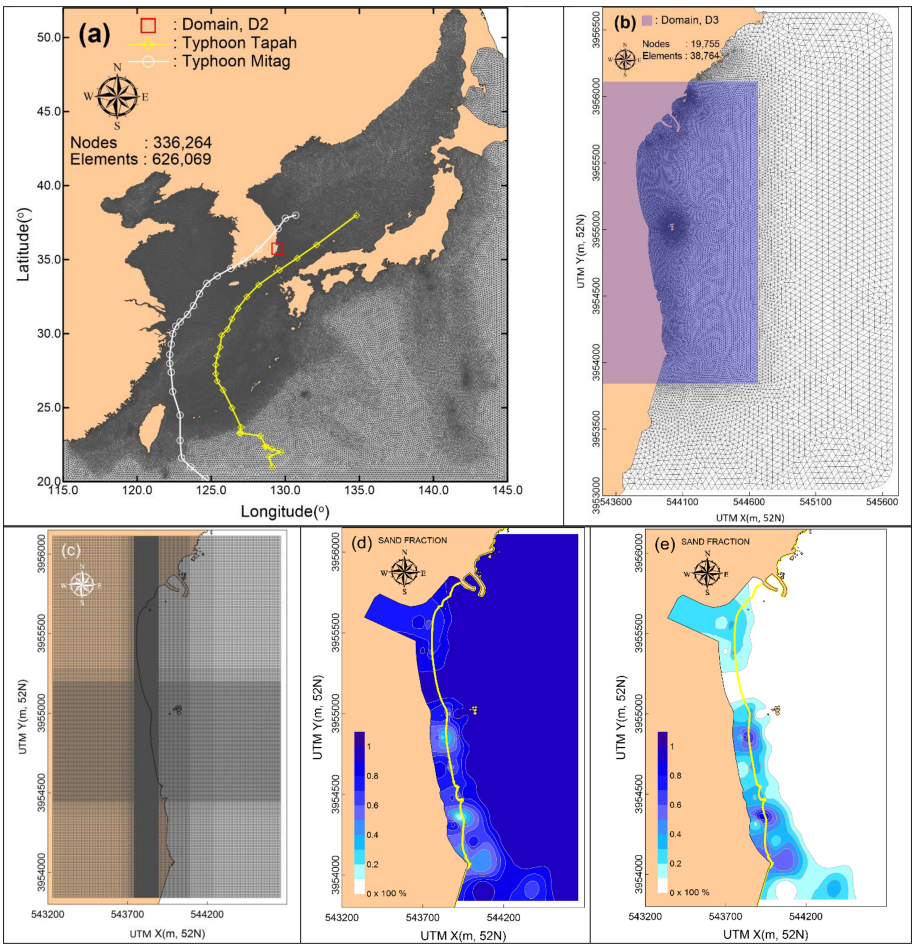

FIGURE 8 | (A) Computational domain and the unstructured meshes in the computational domain, D1, for Telemac-2D. The paths of Typhoon Tapah (yellow) and Mitag (white) are added in **Figure 10A**. **(B)** Computational domain and the unstructured meshes in the computational domain, D2, for Telemac-2D, **(C)** computational domain and the multi-size grids in the computational domain, D3, for XBeach surfbeat **(D)** distribution of sediment for XBeach run over D3 for the erodible area with sand fraction, and **(E)** erodible area with gravel fraction. The yellow and red solid lines in **Figures 8D**, **E** mark the shoreline positions.

the forcing at the boundaries. The computational domain of D2 included the Bonggil Beach and extended to cover a cape in the northern end and the bank of WNPP in the southern end, with the domain size of 2.02 km by 3.58 km in the cross-shore and the longshore direction respectively (**Figure 8B**). The grid system in D2 used 19,755 nodes and 38,784 elements. The purpose of the run over D2 was to provide the forcing conditions for the final XBeach run over the smallest domain, D3. Therefore, the setup of the model was basically same as that over the domain D1 as it was to produce the tide and wave parameters with finer grids within the domain. One difference was that the time-varying conditions along the D2 boundaries were obtained from the outputs of the run over the domain D1, instead of using the wind and air pressure fields. The model was run for Exp. 1 and Exp. 2 as well, corresponding to the D1 runs. The time step was 2 sec for the tide simulation and 10 sec for the wave simulation using Tomawac.

Once the model data using Telemac-2D were obtained, the XBeach surfbeat was run over the smallest domain, D3, using the results from the D2 run as the forcing conditions along the boundaries. The computational domain just covered the Bonggil Beach with the size of 1.43 km by 2.27 km in the cross-shore and longshore direction, respectively (**Figure 8C**). The XBeach model used a multi-grid system to employ finer grids in the middle of the beach and along the shore. The sizes of coarse grids were 307 m and 217 m in the cross-shore and longshore direction, respectively. The sizes of the fine grids ranged from 2.5 m and 10 m (**Figure 8C**). Along the lateral boundaries, the outputs of Telemac-2D run over D2 were applied to provide the forcing conditions. The model was also run for two experimental cases. First, Exp. 2 was run for 37 days from September 15, to October 21, 2020, for model validation. Once it was validated, the model was run to simulate the shoreline changes during Typhoon Tapah and Mitag in Exp. 1. For XBeach surfbeat, semi-empirical parameters were determined for the default settings (Roelvink et al., 2009). The parameters were re-determined based on the laboratory and field measurements from the WTI 2017 (Wettelijk Toets Instrumentarium) project (Van Geer et al., 2015), which were also employed for the two experiments in this study.

In the model, the sediment size could be input differently at each grid point. In addition, two different values of D50s (one for sand and the other for gravel) could be input considering the proportion of each at each grid point. As described earlier, the proportions of the sand (including silt and clay) and gravel were measured at all of the 72 sediment sampling locations, as shown in the new figure (**Figure 2B**). This proportion data have been interpolated/extrapolated in all model grid points, as shown in **Figures 8D**, **E**. Therefore, at each grid point, the fraction of sand and gravel was determined, giving 100% when the two proportions were added. At each grid of the model, the sand (D50 = 0.44 mm) and gravel (D50 = 2.34mm) sizes were input considering the sand and gravel fraction. For example, at the grid point that contained the sampling location B20, there were 4 input parameters for the sediment size as 1) D50_s = 0.44mm; 2) D50_g = 2.34mm; 3) Proportion_Sand = 86.75%; 4) Proportion_Gravel = 13.25%.

4 RESULTS

4.1 Model Validation

The performance of Telemac-2D with Tomawac is examined using the wave measurements at A1. **Figure 6** compares the significant wave heights (H_s), peak wave period (T_p) and wave propagation direction (D_p) between the observation and model data for both Exp. 1 in 2019 and Exp. 2 in 2020. The results show that all three wave parameters were well reproduced by the model during most of the time in both Exp. 1 and 2. Specifically, the modeled H_s nicely agreed even during the storm periods when the maximum H_s reached ~7 m at the time of Typhoon Tapah. During Exp.2, the storm waves (maximum $H_s > 2$ m) were observed two times around September 27 and October 9, 2020. Although the maximum wave heights during the storms in Exp. 2 were lower than those during the storms in Exp. 1 as H_s reached ~2.7 m on September 27 and ~4.0 m on October 9, their periods were longer compared to those in Exp. 1. Considering that the storm impact on sediment transport could increase with storm duration (Almar et al., 2010), it was expected that morphological changes would also be significant during Exp. 2. However, the erosional damage was much weaker for Exp. 2, even though there were two additional typhoons that had greater intensity, Mysak (September 3, 2020; Category 4) and Heishen (September 8, 2020; Category 4), consecutively affiliated the site just before Exp. 2 started, which is discussed in the next section. The modeled wave period, T_p, also nicely matched the observation data except for when T_p abruptly changed. In the case of the wave direction, there were times when the measured data were widely scattered, which was likely due to instrumental error. Except for those times, D_p was also nicely agreed between the two data sets.

Both of the Telemac-2D and XBeach surfbeat model results were also validated through comparison with the hydrodynamic measurements from Exp. 2 (it is noted that the hydrodynamic data were not available for Exp. 1). In **Figure 9**, the longshore (U) and cross-shore (V) velocity measured at B1 during Exp. 2 are compared between the observation and model data. Usually, the velocity magnitude was small as the fluctuation by tidal currents was dominant with a range of ±0.1 m/s in the cross-shore direction, except for the time when the maximum longshore current speed increased up to ~0.5 m/s on October 9, 2020, during the attack of storm waves with maximum H_s of ~ 4 m. In this time, the model result by Telemac-2D was underestimated with a maximum longshore current speed of ~0.2 m/s, whereas XBeach surfbeat was overestimated as its speed reached ~0.7 m/s. Except for this peak, however, the longshore currents were generally in good agreement with the observation with XBeach surfbeat. In the cross-shore direction, the error by Telemac-2D was greater as the current direction was opposite on October 8 – 9, 2020, compared to that by XBeach surfbeat which showed better agreement with the measured data in this period. The better performance in XBeach surfbeat is confirmed in the bottom panels of **Figures 9A**, **B** in which the velocity magnitude was compared between the two models and the observed data, focusing the storm period from October 6, 2020 to October 12, 2020. It shows that the maximum value of current speed of ~0.5 m/s could be modeled by XBeach surfbeat whereas it was

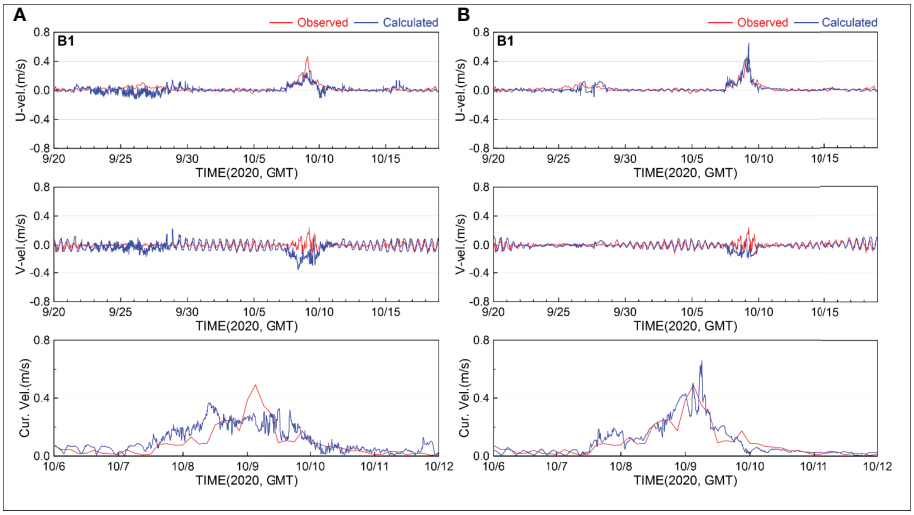

FIGURE 9 | Comparison of measured (red) and model (blue) data between **(A)** Telemac-2D, and **(B)** XBeach surfbeat using the velocity measurements in Exp. 2. Top: longshore (*U*) velocity components (+: north); middle: cross-shore (*V*) velocity components (+: offshore); bottom: velocity magnitude during the storm period from October 6, 2020 to October 12, 2020.

underestimated by Telemac-2D. It is also noted that the tidal currents were more accurately simulated by XBeach surfbeat because the Telemac-2D was slightly overestimated in most times when the tide was dominant. Considering the comparison results, it was concluded that the XBeach surfbeat showed better performance in generating the nearshore currents at B1 during Exp. 2. It is noted that the model errors in simulating the flows are likely because these 2-D models provided depth-averaged flow velocities whereas the observation data were measured near the bottom so that the vertical variation of flow structure could not be calculated by the models. The statistics of the model data such as the root mean square error ($\mathrm{RMSE} = \sqrt{\langle (x_c - x_m)^2 \rangle}$) and BIAS= ($\langle x_c - x_m \rangle$) for the sea surface elevation and the longshore and cross-shore velocities at B1 are listed in **Table 2**.

Once the hydrodynamic data were validated, the next step was to validate the XBeach surfbeat in simulating the morphological change (it is noted that Telemac-2D was used to provide forcing conditions for XBeach surfbeat, and not used to calculate morphology change). In **Figures 10A**, **B**, the morphological changes obtained from bathymetry measurements on September 17 and October 21, 2020 are compared with those calculated by XBeach surfbeat during Exp. 2 from September 15 to October 21, 2020. In general, the model reasonably generated the pattern of morphological change during the period, as shown in the green rectangles of the figure. For example, both of the severe erosions in L0, at the outer part of the breakwater, and L2, in the lee area of the island 'MunMu-daewang-neung', was nicely simulated by the model. In addition, the seabed erosion in in the southern part of the beach in L4 was also in an agreement between the observation and model data, which confirms the validation of XBeach surfbeat in simulating the morphology in general. However, there are areas where there were discrepancies if compared in detail. For example, the beachface in the northern part (L1) were deposited by the observation but eroded by the model. In addition, the erosion and deposition pattern in L3 and L5 occurred oppositely between the model and observation. In order for the additional validation of the model, the beach profiles calculated by XBeach surfbeat model are compared with the observation along the line marked in **Figure 10C** on two days in 16 September and 21 October, 2020 (**Figures 10D**, **E**). It was observed that there were dramatic changes in the bottom topography in the nearshore during the period, but the model nicely reproduced this rapid change. For example, a pit was observed just seaside of the shoreline with maximum depth of ~8 m in 16 September 2020, which was recovered in 21 October, 2020, which was successfully simulated by the model. The pit was formed in the edge of the salient located in the lee of the island before the attack of the storm (**Figure 10C**). After the storm, however, the salient moved to the south (yellow line in

TABLE 2 | Validation by statistics at B1.

Xbeach				**Telemac-2D**			
	Elevation(m)	**U-vel.(m/s)**	**V-vel. (m/s)**		**Elevation(m)**	**U-vel. (m/s)**	**V-vel. (m/s)**
RMSE	0.063	0.037	0.051	RMSE	0.057	0.048	0.072
BIAS	0.004	-0.001	-0.005	BIAS	-0.002	-0.010	-0.021

Figure 10C) and the pit was filled. The profiles in **Figures 10D, E** show that this process was reasonably simulated by Xbeach surfbeat. The model results also quantitatively agreed with the measured data. However, the model accuracy decreased at the nearshore area outside the pit (x = 543880 – 543950 m) where the modeled seabed topography in October, 2020 was lower than the observation with maximum discrepancy of ~2 m.

The model validation based on the data in Exp. 2 might not correctly reflect the damages in Exp. 1 in 2019 because the severe damages (e.g. dune erosion in the southern part) by Typhoon Tapah in 2019 were not recovered in Exp. 2. As shown in **Figure 10A**, however, the seabed morphology was also significantly changed during Exp. 2. In addition, the profiles in **Figure 5B** show that the seabed could be significantly changed after Typhoon Tapah until Exp. 2 started in 2020, which indicates that the seabed was adjusted for ~1 year since Tapah in 2019. Therefore, the seabed changes observed in Exp. 2 was mainly occurred during the period of EXP. 2 once the seabed morphology was considerably adjusted after Tapah, thus the data measured in Exp. 2 was still effective for the model validation.

4.2 Simulation of Shoreline Retreat in 2019

In this section, the results by XBeach surfbeat for Exp. 1 in 2019 are presented. The model was run for two cases during Exp. 1. In the first case, it was run from September 15 to September 24, 2019 so as to identify the impact of Typhoon Tapah only and to exclude the impact of Typhoon Mitag by stopping the model before the event of Mitag. In the second case, the model was run from September 15 to October 3, 2019 so that the impacts of both Tapah and Mitag was considered. **Figure 11** compares the results of morphological changes between the two cases. Although minute differences are observed, the two results are basically the same, which indicates that the significant morphological changes captured in **Figure 3** were caused by Tapah only, and the impact by Mitag was not significant in this site.

The similar model results of morphological changes between the two cases supported the witness from the dwellers in the study area, as mentioned in Section 2.2, that the severe damages in the southern part of the beach was observed just after Typhoon Tapah. If that is the case, the reason that Typhoon Mitag did not make significant impacts in the nearshore morphology needs to be explored. One of the direct indications was the discrepancy in the wave height between the two typhoons. As shown in **Figure 4**, the maximum H_s reached ~7 m during the attack of Tapah whereas it was less than 4 m during Mitag. Therefore, the wave energy that proportional to the square of the wave height would be higher in the study site during Tapah than Mitag. However, it should be also noted that the wave energy during Mitag was likely high enough to cause the erosions. As shown in the wave rose in **Figures 2C**, **D**, more than 90% of wave height were less than 2 m in this area. Therefore, the maximum wave height of ~4 m during Mitag could provide sufficient wave energy to cause erosions. For example, the data measured by a video monitoring system confirmed that the shorelines in another beach in the eastern coast of the Korean Peninsula (i.e. the beach with similar wave conditions with Bonggil Beach) significantly changed when the storm waves with maximum H_s lower than 4 m attacked the site (Oh et al., 2021). This unusual phenomenon was likely related with the recovery process. Once severe erosion occurred during Typhoon Tapah, the beach was gradually recovered under milder wave conditions followed by the storm (Hsu and Hanes, 2004), and the time that was required for the recovery could take months or even years (Forbes et al., 2004; Ranasinghe et al., 2012; Vousdoukas et al., 2012; Morales-Márquez et al., 2018). Therefore, it was likely that the severely eroded condition resulted from the attack of Tapah would not be recovered yet when Typhoon Mitag attacked the site again ~10 days later. Therefore, the impact by Typhoon Mitag whose wave energy at Bonngil Beach was relatively lower than that of Typhoon Tapah could not be sufficient to cause additional erosion. This result indicates that, in analyzing the storm impacts and planning the mitigation/adaptation measures, it is important to consider the resilience of the beach recovery in the study site, which will be revisited in the discussion section 5.1.

Although the model result of the morphological change by XBeach surfbeat could not be verified due to the lack of observation data during Exp. 1, the severe erosion in the southern part of the beach (**Figure 3**) was successfully simulated by the model as shown in the green rectangle, L6, in **Figure 11**. However, the model result also shows some errors because it was overestimated for the dune erosion. Although the erosion generally occurred along the beachface of the beach, it was less severe when compared with that simulated by the model, especially in the areas marked by rectangles L7 and L8. Therefore, the model results were likely exaggerated even though the general pattern of dune erosion was in agreement with the observations, which is discussed in the next section. The reason for the model's overestimation was still unclear. However, one of the factors that could affect the model results was the sediment size. As shown in **Figures 2A**, **B**, the beachface of Bonggil Beach was covered by a mixture of sand and gravel. Although gravels are more stable than sand in starting the incipient motion due to the gravity, they could be more active in motions once started and the fraction of sand and gravel in **Figures 8D**, **E** could be a controlling factor that determined the amount of eroded sediments. However, the model input in **Figure 8** was determined by the field survey during Exp. 2, which might be different from the sediment distribution during the time of Typhoon Tapah and Mitag (Exp. 1). Therefore, the insufficient information on the sediment distribution for the sand and gravel mixture possibly contributed to the overestimation of dune erosion along the beachface.

4.3 Simulation With Coastal Structures

The goal of this study was to develop a plan that can be used to protect the beach from future damages by similar or even more severe storm attacks. To achieve this goal, we tested three cases of model runs to examine the effectiveness of coastal structures as engineering measures. For the engineering structure, submerged breakwater (SB) and submerged groin (SG) were used as they have been commonly used for the hard structures on the east coast of South Korea. The first case (**Case 1**) was to place an SB in front of the northern part of Bonggil Beach (**Figure 12B**). This

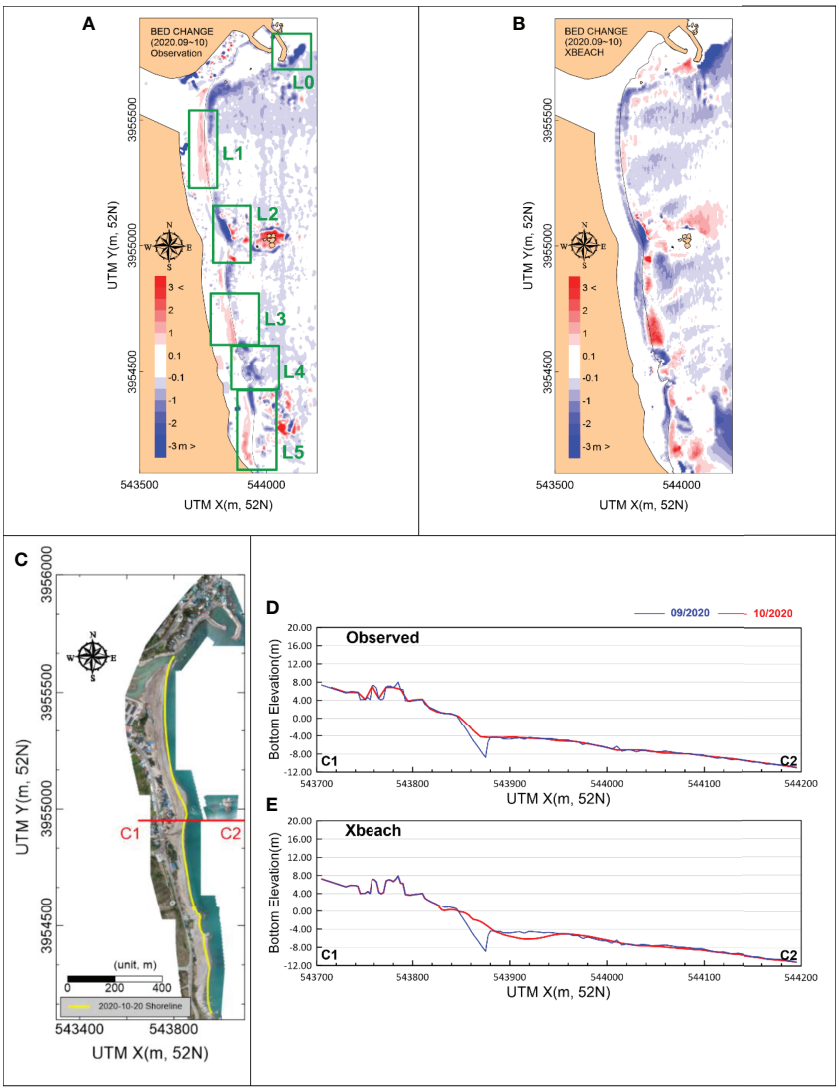

FIGURE 10 | Comparison of the **(A)** observed and **(B)** modeled morphological changes for Exp. 2. The observation data were obtained by the bathymetry measurements on September 17 and October 21, 2020. The model data were calculated by running XBeach surfbeat from September 15 to October 21, 2020. The green rectangles, L0 – L5, in the left panel mark the areas where the morphological change was in agreement or in disagreement between the observation and model data, **(C)** map of the site measured by the drone on September 10, 2020, before the attack of the storm. The yellow line on the map was the shoreline measured after the storm (October 20, 2020), showing that the salient formed behind the island moved to the south. The red line from C1 to C2 is a beach profile line selected for comparison between observational and modeled bottom topography, **(D)** beach profile measured in 16 September (blue) and 21 October (red), 2020 along the line from C1 to C2 in **(C**, **E)** beach profile calculated by XBeach surfbeat in September (blue) and October (red), 2020 along the line **(C)**. The pit formed in the edge of the salient before the storm attack was filled as shown in **(C)**, which was nicely simulated by the model as shown in **(E)**.

was a direct measure to protect the northern part of the beach. Although the erosion was more severe in the southern part, this plan was considered to protect the facilities that were mostly located in the northern part. The second plan (**Case 2**) was to place a SB in front of the southern part of the beach (**Figure 12C**), which was a direct measure to protect the southern part where severe erosion occurred. The third plan (**Case 3**) was to place a SG at the southern end of the beach (**Figure 12D**). This was an indirect measure for the beach protection because the SG would be used to capture the sediments that could leave the coastal cell of the beach by erosion instead of directly preventing the erosion. In fact, additional cases might be designed for the model simulation, and the performance of all cases could be compared by calculating the effectiveness in numeric. However, this type of effectiveness could not be verified without observation data to prove it. Therefore, we selected the three cases, instead of increasing test cases, because they represented hard stabilization measures that directly disturbed sediment motions and a soft

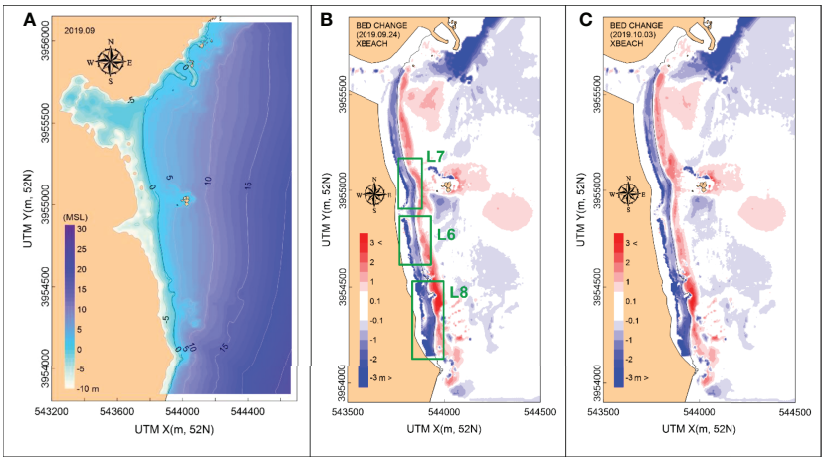

FIGURE 11 | (A) Geographical set up of XBeach surfbeat for Exp. 1, and **(B)** the model result of the morphological change that considered the impacts of Typhoon Tapah only by running the model from September 15 to September 24, 2019, and **(C)** the model result that considered the impacts of both Tapah and Mitag by running the model from September 15 to October 3, 2019.

stabilization measure that could conserve the sediments within the coastal cell.

In **Figure 12**, the model results of the morphological changes by XBeach surfbeat are compared between the three cases of coastal structure arrangement. For all cases, the model was set up with the storm wave conditions used for Typhoon Tapah, and was run for 15 days from September 15 to October 3, 2019 to observe the impacts by Tapah and Mitag with the structures, although Mitag could not make a significant impact. The model results are compared to the case without any structures (**Figure 12E**). For the first case of the run (SB in the northern part, **Figure 12F**), the beach was protected in the northern part as the sediments in the beachface were less eroded, and sediments were deposited in the lee of the SB, as shown in L9 of **Figure 12F**. However, side effects were also observed as the seabed was severely eroded in the north end of the SB (L9). In addition, the seabed in the south end of the SB was eroded (L10), which was not observed in the case of the run without the structure. It is also noted that the eroded sediments were cumulated in the southern end of Bonggil Beach as found in L11.

The side effects of SB were also observed in the second case of the simulation (SB in the southern part, **Figure 12G**). Although the beachface was less eroded, and sediments were cumulated in the lee of the SB as shown in L12, there could be a serious seabed erosion in the southern end of the SB (L13). In addition, the beachface in L13 was more severely eroded than the case without any structure (**Figure 12E**). These eroded sediments were cumulated in the southern end of the beach (L14). In the third case (SG in the southern end of the beach, **Figure 12H**), the side effect was minimal, although the protection of the beachface was also minimal. The erosion pattern in the beachface was similar to the case without structure, which indicates that the beach could not be protected in the future attacks of similar storm waves as Typhoon Tapah. However, the eroded sediments might not be lost from the coastal cell but cumulated in the area around the SG (L15). It is also noted that the sediments were eroded in L16, which was opposite to the findings of other cases because the sediments were cumulated in this area as observed in L14 of **Figure 12G**. This opposite pattern of sediment deposition/erosion is important because this area L16 is located in front of the WNPP and thus outside of the coastal cell. Therefore, the sediments cumulated in this area indicate that they would not return to Bonggil Beach but lost for good. This possibility of sediment loss from the coastal cell might be reduced by constructing the SG as in **Figure 12H**.

The simulation results indicated that the protection of the beach from the loss of sediments in the northern and southern parts could be more effective by constructing the SBs (**Case 1 and 2**). However, these cases might cause significant side effects of additional erosions at the unexpected seabed locations in the nearshore. Considering that these rapid seabed erosions were caused in a short-term period (days) during an attack of the harsh storm such as Typhoon Tapah, they could lead to longer-term (months) erosions in other parts of the nearshore areas when the post-storm process occurred to reach an equilibrium status. In contrast, the use of SG (**Case 3**) might have results with lower performance in directly preventing the severe erosion in the southern part of the beach. However, the side effect of unexpected seabed erosion would be much reduced. In addition, the loss of total sediments within the littoral cell could be reduced by preventing the outgoing sand movement through P4, by using the SG to save the transported sediments around it. Therefore, we suggest that **Case 3** as a favorable measure out of the three cases. Considering the goal of this study to protect the beach from future storm attacks, the possibility of additional erosions due to SBs would make it hesitant to choose the plans by **Case 1** and **2** because it would be no remedy because the SBs would only switch the locations of erosion if the additional erosions were to occur at other unexpected nearshore locations. Although recommended, it is noted that **Case 3** is still not be a perfect protection plan

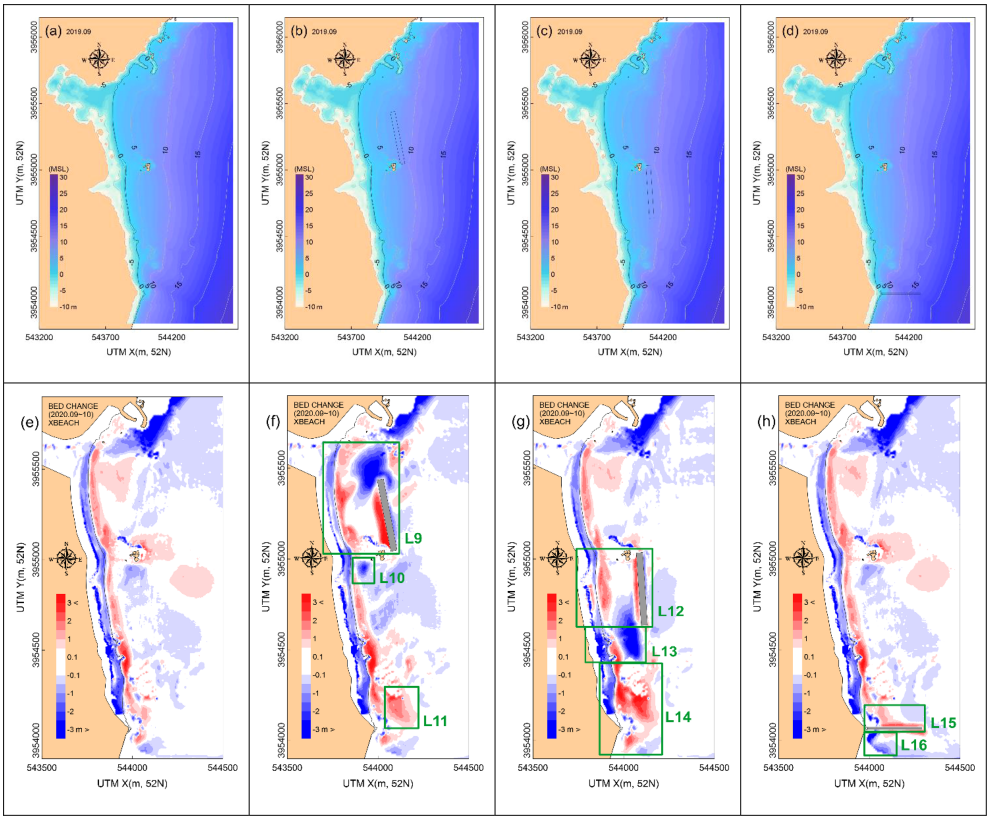

FIGURE 12 | Plan view of the test cases for simulation with coastal structures, **(A)** without structure, **(B)** with a submerged breakwater (SB) placed in front of the northern part of Bonggil Beach, **(C)** with a submerged breakwater (SB) placed in front of the southern part of the beach, **(D)** with a submerged groin (SG) placed in the southern end of the beach, and comparison of model results of morphological changes by XBeach surfbeat for the four different cases, **(E)** without structure, **(B)** with a SB placed in front of the northern part of Bonggil Beach, **(C)** with a SB placed in front of the southern part of the beach, **(D)** with a SG placed in the southern end of the beach. The model was run for 15 days from September 15 to October 3, 2019 that included the impacts of Typhoon Tapah and Mitag.

for the beach as it could still cause dune erosion in the southern part of the beach. Considering previous studies, hard structures might increase coastal variability and could worsen erosion (van Rijn, 2011; Do et al., 2021a). Therefore, measures that could conserve the equilibrium condition should be more desirable in preventing unexpected side effects.

5 DISCUSSION

The primary goal of the present study was to find out a measure to protect the beach by mitigating the erosional damage from future attacks of storm waves. For this, it was important to carefully analyze the causes of the erosional damages by the storm waves. One of the most significant observations in terms of the erosion during Typhoon Tapah and Mitag in 2019 was the discrepancy in the damage between the southern and northern parts of the beach as it was more severe in the southern part. As observed in the previous sections, the direct reason for this discrepancy was the difference in the water depths between both sides as the seabed was steeper in the nearshore area of the southern part. Due to the shoaling of the propagating waves, the wave energy dissipation was greater in the northern part, whereas more energy could be focused in the southern part, causing the severer damage. The reason for this difference in the bathymetry can be found in the characteristic pattern of geography in Bonggil Beach. The mouth of Daejong Stream was located in the northern part, and thus the sediment input through the stream was focused in this area (P2 in **Figure 1B**). In addition, the island, 'MunMu-daewang-neung', located in the middle of the beach (P3) and the salient in the lee area of P3 likely disturbed the movement of the input sediment to the southern part, which has resulted in the discrepancy in the bathymetry between the two parts. Besides the natural cause, there might be an anthropogenic factor as well that contributed to the bathymetry difference. As shown in **Figure 1B**, the artificial bank (P5) was built to protect the WNPP, which has deepened in the front area of P5 as shown in **Figure 7A**. Therefore, the sediments in the southern part would not return to this area if they were transported to the P5 area through P4, which was confirmed by the XBeach surfbeat simulations shown in L14, L15, and L16 of **Figure 13**. L14 shows that the sediments were transported to P5 through P4 during the

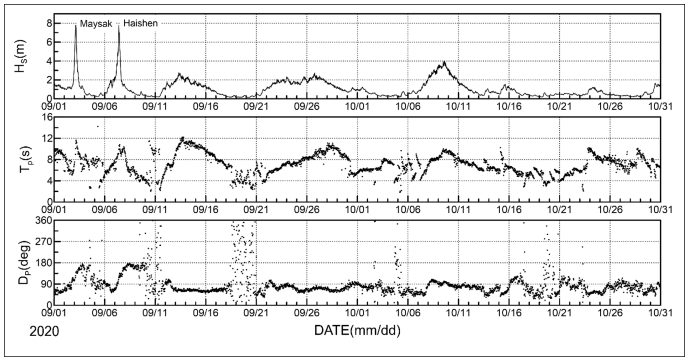

FIGURE 13 | Time series of significant wave height (H_s), peak wave period (T_p), and peak wave direction (D_p) for two months from September 1 to October 31, 2020, covering the times of Typhoons Maysak and Haishen, measured by the AWAC at A1. It is noted that Exp. 2 started on September 15, 2020, after these typhoon events.

storm attack which might not be recordable, and L15 and L16 indicates that the sediments were protected within the coastal cell with construction of the submerged groin.

As for the numerical model results, XBeach surfbeat simulated the pattern of erosion with reasonable agreement. In terms of the quantity, however, the model overestimated the degree of erosion in both experiments of Exp. 1 in 2019 and Exp. 2 in 2020. The reason for this has not been clearly understood yet. As described previously, the sediment input data might be correctly obtained as they were elaborately sampled at 72 locations inside/outside the water, which turned out that gravels were mixed with sand. XBeach model possibly had lower accuracy when the bottom was covered by the gravel of much larger size than sand (D50 = 0.44 mm sand and 2.34 mm for gravel). There have been numerous studies to run the XBeach model in the sandy beds so that the model could have been correctly tuned for sand. However, the studies for gravel beds was relatively rare as described in the introduction. Therefore, the model setup for gravel beds could show less accuracy. One of the ways to check this was to use 1-D XBeach-G model to apply in the gravel beach, similar to the previous researches by Jamal et al. (2014) & McCall et al. (2015), and to compare the results with observation data. In case the model performance becomes lower for the gravel beach, then the model setup could be tuned to increase the accuracy. Then, the new setup can be applied in Bongil Beach using the 2-D Xbeach surfbeat model, which is planned for a future study.

In addition to the understanding of the erosional process during the storm events, it is also necessary to compare the impacts of storm waves between different typhoon events so as to develop an effective measure considering the diversity of various storm conditions. For example, there was a discrepancy in the storm damages done by the typhoons in 2019 and 2020. As described in the previous sections, the damage in the study site was greater by the attacks of Tapah (and additionally by Mitag) in Exp. 1 of 2019 than that by the storm waves in Exp. 2 of 2020. Although the wave heights of the storm waves in Exp. 2 were lower than those in Exp.1, their durations were longer (**Figure 6**), which might be an important factor for nearshore morphological changes as well (Almar et al., 2010; Coco et al., 2014; Do et al., 2021b). For example, Almar et al. (2010) analyzed the data of a double-sandbar system in Truc Vert Beach, France. During their two-month observational period, four storms attacked the site. The pre-existing crescentic sandbar system was straightened and migrated offshore ~100 m by the severest second storm with maximum H_s of ~8 m. However, significant changes in the bar system also occurred during the longest fourth storm of ~10 day duration and H_s of 2 – 4 m as the bar developed crescentic pattern and migrated ~200 m southward. Similarly, Coco et al. (2014) suggested that the duration of consistently large waves and their effect on beach morphodynamics made the event comparable to an extreme storm. In addition, Do et al. (2021b) observed that a crescent sandbar system was fully developed from a straight sandbar system, during the longer second storm of ~6 day duration and maximum H_s of ~4 m, rather than during the stronger first storm of ~2 day duration and maximum H_s of ~5 m, which indicates that the duration of storm waves might play role in changing nearshore seabed morphology. Although direct comparison was not possible, the longer storm durations in Exp.2 than Exp. 1 could provide a favorable condition for additional erosion in Bonggil Beach but it did not occur, which will be further discussed later in this section.

It is also noted that two typhoons (Typhoon Mysak and Heishen) consecutively attacked the site just before the period of Exp. 2 (Mysak on September 3, 2020; Heishen on September 8, 2020). Considering that both Mysak and Heishen were Category 4 storms (Tapah and Mitag were Category 1 and 2 storms, respectively), the impacts by Mysak and Heishen would have been significant as their H_s measured in A1 was greater than that by Tapah (**Figure 13**). In addition, a favorable condition to morphological change was also observed under a series of storm events (Vousdoukas et al., 2012; Morales-Márquez et al, 2018; Rutten et al, 2018), which corresponds to the case of Mysak and Heishen. However, the erosional damage during Exp. 2 was much less than that during Exp. 1, and the significant discrepancy in the erosional damage between Exp. 1 and Exp. 2 was still unexpected, and additional investigation might be necessary.

One of the other factors to consider was the wave propagation direction. Although the amount of total sediment transport

depends on the wave power that is contributed by the wave height and period (Oh et al., 2021), the ratio between the cross-shore and longshore transport may be related to the wave direction, and it can result in the locality of erosional process, especially in the beaches with complex geography such as Bonggil Beach. The results in **Figure 4** show that the waves were approaching the shore in E direction (~82°) consistently for ~3 days during Tapah. In contrast, the wave propagation direction rapidly changed from ENE (60°) to SE (140°) during the course of both Mysak and Heishen. Therefore, the consistency of the wave direction during the storm event might be important in causing the coastal erosion, which requires further analysis in future studies.

Another factor that may contribute to the discrepancy between 2019 and 2020 events is the resilience of the beach for recovery. As described in the introduction, it is a natural process that beaches would be recovered after erosion due to onshore sediment motions under mild wave conditions (Hsu and Hanes, 2004). This recovery process usually took a longer time than the erosional process that occurred within a short-time scale in days during the attack of storm waves, as observed in this study. Previous studies suggested that the temporal scale of the recovery process was various from days to years or even to decades. The factors that affected the recovery process could be coastal morphology, wave energy, shoreline orientation, nearshore circulation, and local sediment supply. For example, individual large storms could cause local rapid erosion from which recovery might take years or even decades if the impacts were large but sand supply after that was not sufficient (Forbes et al., 2004). As for other cases, the recovery process could take months with slower paces of the recovery than the erosion. Vousdoukas et al. (2012) observed that sub-aerial beach volume reduction was up to 30 m^3/mon in steep-sloping beaches whereas the following recovery of the intertidal area was reaching ~10 m^3/mon. Morales-Márquez et al. (2018) found out that a group of storm waves generated significant erosion in three days but only half of the sediment was recovered during the next two months. In contrast, Ranasinghe et al. (2012) analyzed video monitoring data and wave measurements to quantify the nearshore morphological recovery time scale, T_{mr} and observed that T_{mr} could be as short as 5 days in Duck in North Carolina, United States. This result showed that the wave conditions and longshore current developed after the storms could be important indicators for T_{mr} In addition to the hydrodynamic conditions, the antecedent morphological condition could be a crucial factor for the recovery process as the beach might respond quite differently to the same hydrodynamic input conditions, depending on the morphodynamic status. For example, storm attack on susceptible beach could lead to catastrophic breakdown that might not be reversible or require long time for recovery (Forbes et al., 1995). Morales-Márquez et al. (2018) observed that, when a sequence of storms affiliated the beach, the storms developed later could hardly affect the morphology although their intensity was similar to the former ones that caused damages, confirming that the antecedent morphological condition might be crucial for the response of the beach. The antecedent condition could be also applied in the Bonggil Beach when Typhoon Mysak and Heishen attacked the site in 2020. The severe damage by Typhoon Tapah in 2019 might not be recovered and the morphological condition in the beach was not favored for additional erosion when the two severe typhoons affiliated the site again in ~1 year later. The temporal scale of the recovery process has not been estimated in Bonggil Beach yet. However, a similar observation was made in Yeongildae Beach that is located ~35 km north of Bonggil Beach (Oh et al., 2021), in which it took ~1.5 yrs for the shoreline of the beach to be recovered back to the level before the time of Typhoon Tapah's attack. Considering that Yeongildae Beach is located inside a bay, and thus the damage by Tapah was smaller than that in Bonggil Beach, it is likely that Bonggil Beach was still in the recovery process when Typhoon Mysak and Heishen affiliated the site in 2020, which was also clear from the profile measurement in **Figure 5B**. Therefore, the less erosional damage during the attack of Mysak and Heishen was likely because the beach was still in the recovery process, and the antecedent morphological condition was not favorable for additional erosions at the time of 2020 typhoons.

In designing the long-term mitigation/adaptation plans from extreme storm impacts in the study area, it is important to carefully consider the post-event recovery processes in order to reduce unexpected/unwanted side effects that might be caused by the implementation of the plan. The decision from the simulation results in Section 4.3 were based on such consideration. Out of the three cases, **Case 3** that planed the SG to conserve the sediments within the coastal cell was suggested for a preferred measure whereas **Case 1 and 2** that planned SBs were not suggested due to the predicted additional erosions in the unexpected nearshore locations. Because the hard stabilization structures of SBs would not only reduce the wave energy but they also directly block the cross-shore sediment motions, they could also disturb the post-event recovery process by blocking the onshore sediment movement under milder wave conditions. In addition, such plans can be designed more economically if both destructive (erosion by storms) and constructive (post-event recovery) processes are considered, than those that only consider the destructive process. For example, the plan by **Case 3** could also be economical when comparing the initial costs that were required in constructing the coastal structures. For example, the cost to construct the SG by **Case 3** would be cheaper than those to construct the SBs by **Case 1 and 2** because the SG would not need to be built high above the seabed, whereas the SBs should be high and wide to effectively reduce the wave energy. The plan by **Case 3** could be also economical because the sediments were conserved in the nearshore area without losing them from the littoral cell and they could be replenished back to the eroded area. However, the outcome of this study suggests that the considerations on the mitigation/adaptation from storm impacts should be confined in the study area. One of its reasons is that the resilience of post-storm recovery could be site-specific, as previously discussed, even under similar hydrodynamic and wave conditions, thus studies are required to be carefully conducted for specific site in developing mitigation/adaptation plans from storms.

One of the examples of such studies was done for Miami-Dade County, United States (Klima et al., 2012). In this research paper, hurricane adaptation plans to reduce damages from the attack of

tropical cyclones were developed by calculating surge height and wind speed as a function of return period and by estimating costs and economic losses using a damage model, for five areas along the county's coastline. In particular, the study noted that the five areas would have different susceptibilities even to same hurricane due to different bathymetry/topography and infrastructure. Therefore, the plans were developed site-specifically for each area by suggesting, for example, a surge barrier as the best method to reduce storm surge damage in one area but suggesting the best method to be varied with return period in another area. This result corresponded to the suggestion in the present study that such adaptation plan should be considered specifically for different site. In Bonggil Beach, a coastal management project was planned by the local government before the severe erosion damages by Typhoon Tapah occurred in 2019. According to this plan, a SB was designed to be placed in the northern part of the beach's nearshore, similar to the second plan (Case 2) shown in **Figure 12B**, to protect the commercial places located behind the northern part. Once Tapah affiliated the beach, however, the plan might require modification to consider beach conservation/adaptation from storm attacks. The results of the present study were then provided to suggest a design of engineering structure for future conservation specified in Bonggil Beach, considering the beach's characteristic pattern.

6 CONCLUSION

In the present study, field observations and numerical model experiments were carried out to analyse the severe erosion in the beachface of Bonggil Beach during the attack of Typhoon Tapah in September 2019. The models were validated with a reasonable agreement with observational data. Telemac-2D showed good performance in generating the wave conditions during both of the 2019 (Exp. 1) and 2020 (Exp. 2) experimental period. When comparing the Telemac-2D and XBeach surfbeat, XBeach showed better performance because the measured current data were more accurately generated by Xbeach surfbeat than Telemac-2D. The morphological changes simulated by the XBeach surfbeat for Exp. 2 were also agreed with the bathymetry measurements in general. However, the model overestimated the degree of erosion because the amount of modeled sediments that were eroded from the beachface was greater than that measured from field observation. The reason was likely due to the complicated sediment characteristics as the sediment in Bonggil Beach was a mixture of sand and gravel. To implement the impact of this sediment mixture in the model, the sand and model fraction of the erodible sediment part was elabolately determined based on the sediment samples obtained at 72 locations along the beachface and inside the water in the nearshore. However, the existence of gravel whose size (1.34 mm) was much larger than that of sand (0.44 mm), which might increase the simulation error. Considering that the gravels would be more stable in starting initial motion but more active once started the bedload motions, the errors in the sand/gravel fraction in the model setup might lead to the wrong estimation of the amount of eroded/deposited sediments, although the pattern their distribution was successfully simulated by the model.

The application of the XBeach surfbeat for the Typhoon Tapah event for Exp. 1 also resulted in general agreement of the sediment transport pattern even though the model also overestimated the degree of erosion along the beachface. In particular, the locality of the erosional pattern, the severe dune erosion in the southern part, was successfully simulated by the model. The locality was caused because the slope of the water depth was steeper in the southern part, which likely kept the propagating wave energy higher when reaching the shore during the attack of Typhoon Tapah. In Bonggil Beach, the sediments were input to the coastal cell from a stream connected to the northern end of the beach. However, the input sediments could have hardly reached the southern part due to the blocking of the island, 'MunMu-daewang-neung', located in the middle of the beach. In addition, the sediments in the southern part could not return to the coastal cell once they crossed the southern boundary of the beach. It was because the water depth outside the boundary was deepened due to the construction of the bank in front of a nuclear power plant. Due to the combined effect of natural and anthropogenic causes, the nearshore of the southern part of the beach has been kept deeper than that in the northern part, causing the locality in the erosional damage.

Additional simulations with three cases of engineering measures were performed in order to find out an effective measure in protecting/conserving the beach from future attacks of similar storm waves – construction of a submerged breakwater (SB) in front of the northern part of the beach; construction of a SB in the southern part; and construction of a submerged groin (SG) at the southern end of the beach to prevent the loss of sediments from the coastal cell. It turned out that, out of the three measures, the use of SG was most effective in conserving the beach because the two measures with SB might cause the side effect of additional erosions at unexpected seabed locations even though they were useful for directly protecting the shore in the lee side of the SBs. Although the direct impact of dune erosion could not be avoided, the SG would be an environmentally friendly measure with reduced side effects, and by keeping the sediments within the coastal cell around the SG that could be used for future replenishment, even though sediments could be conserved by the SG on specific situations, mainly depending on the wave directions that caused longshore sediment drift. In addition, the construction of SG might require less initial construction cost than SBs because the SG did not necessarily high above the seabed by only capturing the bedload sediments. Considering that the SBs could prevent the long-term recovery process of the onshore sediment motions under milder wave conditions, the measure with the SG was also recommended as it allowed the natural recovery although it was still not a perfect measure in protecting the beach from dune erosion.

One of the restrictions of this study was that its outcomes were site-specific and might not be applied in other areas. However, this study focused the importance of the locality in establishing storm adaptation plans, in even within the same area of the littoral cell. Due to the climate change and the subsequent sea-level rise or the possiblility of increasing storm intensity, it is essential to prepare for long-term adaptaion plans in many coatal regions globally. The result of this study noted that these plans should

consider the characteristic patterns of the site that might include the bathymetry, topography, wave climae, and the resilience of the site for post-storm recovery process. For this, preliminary researches are required to be carefully conducted for the sites of interest, considering their values.

DATA AVAILABILITY STATEMENT

The raw data supporting the conclusions of this article will be made available by the authors, without undue reservation.

AUTHOR CONTRIBUTIONS

JDD, J-YJ, WMJ and Y C contributed to conception and design of the study. JDD, BL, JYC, SKH and KK organized the database. JDD, BL, JYC, SKH and KK performed the statistical analysis. JDD and YC wrote the manuscript. All authors contributed to manuscript revision, read, and approved the submitted version.

FUNDING

This work was supported by the Korea Institute of Ocean Science and Technology [grant number PEA0031], and the Ministry of Oceans and Fisheries [grant number PM62850].

SUPPLEMENTARY MATERIAL

The Supplementary Material for this article can be found online at: https://www.frontiersin.org/articles/10.3389/fmars.2022.825359/full#supplementary-material

Supplementary Table 1 | Information on the sediment samples (sampling location, sediment size and type).

Supplementary Table 2 | Information on the wind and wave parameters during Exp.1. The data measured during the period of Typhoon Tapah are highlighted (21 - 24 September, 2019).

REFERENCES

Almar, R., Castelle, B., Ruessink, B., Sénéchal, N., Bonneton, P. and Marieu, V. (2010). Two-And Three-Dimensional Double-Sandbar System Behaviour Under Intense Wave Forcing and a Meso–Macro Tidal Range. *Continental. Shelf. Res.* 30, 781–792. doi: 10.1016/j.csr.2010.02.001

Anthony, E. J., Brunier, G., Besset, M., Goichot, M., Dussouillez, P. and Nguyen, V. L. (2015). Linking Rapid Erosion of the Mekong River Delta to Human Activities. *Sci. Rep.* 5, 1–12. doi: 10.1038/srep14745

Asaro, G. and Paris, E. (2000). The Effects Induced by a New Embankment at the Confluence Between Two Rivers: TELEMAC Results Compared With a Physical Model. *Hydrological. Processes.* 14, 2345–2353. doi: 10.1002/1099-1085(200009)14:13<2345::AID-HYP33>3.0.CO;2-X

Bender, M. A., Knutson, T. R., Tuleya, R. E., Sirutis, J. J., Vecchi, G. A., Garner, S. T., et al. (2010). Modeled Impact of Anthropogenic Warming on the Frequency of Intense Atlantic Hurricanes. *Science* 327, 454–458. doi: 10.1126/science.1180568

Bergillos, R. J., Masselink, G., Mccall, R. T. and Ortega-Sánchez, M. (2016). Modelling Overwash Vulnerability Along Mixed Sand-Gravel Coasts With XBeach-G: Case Study of Playa Granada, Southern Spain. *Coast. Eng. Proc.* 1, 13. doi: 10.9753/icce.v35.sediment.13

Berkhoff, J. (1973). "Computation of Combined Refraction—Diffraction," in *13th International Conference on Coastal Engineering 1972.)*, Vancouver, Canada, 471–490. doi: 10.1061/9780872620490.027

Coco, G., Senechal, N., Rejas, A., Bryan, K. R., Capo, S., Parisot, J., et al. (2014). Beach Response to a Sequence of Extreme Storms. *Geomorphology* 204, 493–501. doi: 10.1016/j.geomorph.2013.08.028

Davidson-Arnott, R., Bauer, B. and Houser, C. (2019). *Introduction to Coastal Processes and Geomorphology* (Cambridge University Press).

Do, J. D., Jin, J.-Y., Hyun, S. K., Jeong, W. M. and Chang, Y. S. (2020). Numerical Investigation of the Effect of Wave Diffraction on Beach Erosion/Accretion at the Gangneung Harbor, Korea. *J. Hydro-environment. Res.* 29, 31–44. doi: 10.1016/j.jher.2019.11.003

Do, J. D., Jin, J. Y., Jeong, W. M. and Chang, Y. S. (2019). Observation of Rapid Seabed Erosion Near Closure Depth During a Storm Period at Hujeong Beach, South Korea. *Geophysical. Res. Lett.* 46, 9804–9812. doi: 10.1029/2019GL083910

Do, J. D., Jin, J.-Y., Jeong, W. M., Lee, B., Choi, J. Y. and Chang, Y. S. (2021a). Collapse of a Coastal Revetment Due to the Combined Effect of Anthropogenic and Natural Disturbances. *Sustainability* 13, 3712. doi: 10.3390/su13073712

Do, J. D., Jin, J.-Y., Jeong, W. M., Lee, B., Kim, C. H. and Chang, Y. S. (2021b). Observation of Nearshore Crescentic Sandbar Formation During Storm Wave Conditions Using Satellite Images and Video Monitoring Data. *Mar. Geology.* 442, 106661. doi: 10.1016/j.margeo.2021.106661

Forbes, D., Orford, J., Carter, R., Shaw, J. and Jennings, S. (1995). Morphodynamic Evolution, Self-Organisation, and Instability of Coarse-Clastic Barriers on Paraglacial Coasts. *Mar. Geology.* 126, 63–85. doi: 10.1016/0025-3227(95)00066-8

Forbes, D. L., Parkes, G. S., Manson, G. K. and Ketch, L. A. (2004). Storms and Shoreline Retreat in the Southern Gulf of St. Lawrence. *Mar. Geology.* 210, 169–204. doi: 10.1016/j.margeo.2004.05.009

Galland, J.-C., Goutal, N. and Hervouet, J.-M. (1991). TELEMAC: A New Numerical Model for Solving Shallow Water Equations. *Adv. Water Resour.* 14, 138–148. doi: 10.1016/0309-1708(91)90006-A

Gurov, K. and Fomin, V. (2021). Mathematical Modeling the Dynamics of the Bottom Sediments Granulometric Composition in the Balaklava Bay Affected by the Wind Waves. *Phys. Oceanography.* 28, 78–89. doi: 10.22449/1573-160X-2021-1-78-89

Harter, C. and Figlus, J. (2017). Numerical Modeling of the Morphodynamic Response of a Low-Lying Barrier Island Beach and Foredune System Inundated During Hurricane Ike Using XBeach and CSHORE. *Coast. Eng.* 120, 64–74. doi: 10.1016/j.coastaleng.2016.11.005

Hervouet, J. M. (2000). A High Resolution 2-D Dam-Break Model Using Parallelization. *Hydrological. processes.* 14, 2211–2230. doi: 10.1002/1099-1085(200009)14:13<2211::AID-HYP24>3.0.CO;2-8

Holthuijsen, L., Herman, A. and Booij, N. (2003). Phase-Decoupled Refraction–Diffraction for Spectral Wave Models. *Coast. Eng.* 49, 291–305. doi: 10.1016/S0378-3839(03)00065-6

Hsu, T. J. and Hanes, D. M. (2004). Effects of Wave Shape on Sheet Flow Sediment Transport. *J. Geophysical. Research-Oceans.* 109. doi: 10.1029/2003JC002075

Jamal, M., Simmonds, D. and Magar, V. (2014). Modelling Gravel Beach Dynamics With XBeach. *Coast. Eng.* 89, 20–29. doi: 10.1016/j.coastaleng.2014.03.006

Klima, K., Lin, N., Emanuel, K., Morgan, M. G. and Grossmann, I. (2012). Hurricane Modification and Adaptation in Miami-Dade County, Florida. *Environ. Sci. Technol.* 46, 636–642. doi: 10.1021/es202640p

Knutson, T. R., Mcbride, J. L., Chan, J., Emanuel, K., Holland, G., Landsea, C., et al. (2010). Tropical Cyclones and Climate Change. *Nat. Geosci.* 3, 157–163. doi: 10.1038/ngeo779

Masselink, G. and Russell, P. (2013). Impacts of Climate Change on Coastal Erosion. *MCCIP. Sci. Rev.* 2013, 71–86. doi:10.14465/2013.arc09.071-086

McCall, R., Masselink, G., Poate, T., Roelvink, J. and Almeida, L. (2015). Modelling the Morphodynamics of Gravel Beaches During Storms With XBeach-G. *Coast. Eng.* 103, 52–66. doi: 10.1016/j.coastaleng.2015.06.002

Mentaschi, L., Vousdoukas, M. I., Pekel, J.-F., Voukouvalas, E. and Feyen, L. (2018). Global Long-Term Observations of Coastal Erosion and Accretion. *Sci. Rep.* 8, 1–11. doi: 10.1038/s41598-018-30904-w

Morales-Márquez, V., Orfila, A., Simarro, G., Gómez-Pujol, L., Ãlvarez-Ellacuría, A., Conti, D., et al. (2018). Numerical and Remote Techniques for Operational Beach Management Under Storm Group Forcing. *Natural Hazards. Earth System. Sci.* 18, 3211–3223. doi: 10.5194/nhess-18-3211-2018

Oh, J.-E., Jeong, W.-M., Ryu, K.-H., Park, J.-Y. and Chang, Y.-S. (2021). Monitoring of Recovery Process at Yeongildae Beach, South Korea, Using a Video System. *Appl. Sci.* 11, 10195. doi: 10.3390/app112110195

Phillips, B. T., Brown, J. M. and Plater, A. J. (2020). Modeling Impact of Intertidal Foreshore Evolution on Gravel Barrier Erosion and Wave Runup With Xbeach-X. *J. Mar. Sci. Eng.* 8, 914. doi: 10.3390/jmse8110914

Ranasinghe, R., Holman, R., De Schipper, M., Lippmann, T., Wehof, J., Duong, T. M., et al (2012). "Quantifying Nearshore Morphological Recovery Time Scales Using Argus Video Imaging: Palm Beach, Sydney and Duck, North Carolina," in ICCE 2012: Proceedings of the 33rd International Conference on Coastal Engineering, Santander, Spain, Coastal Engineering Research Council, 1–6 July 2012.

Robins, P. and Davies, A. (2011). "Application of TELEMAC-2D and SISYPHE to Complex Estuarine Regions to Inform Future Management Decisions," in Proceedings of the XVIIIth Telemac & Mascaret User Club 2011, EDF R&D, Chatou, 19-21 October 2011. 86–91.

Roelvink, D., Reniers, A., Van Dongeren, A., De Vries, J. V. T., Mccall, R. and Lescinski, J. (2009). Modelling Storm Impacts on Beaches, Dunes and Barrier Islands. *Coast. Eng.* 56, 1133–1152. doi: 10.1016/j.coastaleng.2009.08.006

Roelvink, J. and Van Banning, G. (1995). Design and Development of DELFT3D and Application to Coastal Morphodynamics. *Oceanographic. Literature. Rev.* 11, 925.

Russell, P. E. (1993). Mechanisms for Beach Erosion During Storms. *Continental. Shelf. Res.* 13, 1243–1265. doi: 10.1016/0278-4343(93)90051-X

Rutten, J., Ruessink, B. and Price, T. (2018). Observations on Sandbar Behavior Along a Man-Made Curved Coast. Earth Surf. *Process. Landf.* 43, 134–149. doi: 10.1002/esp.4158

Syvitski, J. P., Vörösmarty, C. J., Kettner, A. J. and Green, P. (2005). Impact of Humans on the Flux of Terrestrial Sediment to the Global Coastal Ocean. *science* 308, 376–380. doi: 10.1126/science.1109454

Van Geer, P., Den Bieman, J., Hoonhout, B. and Boers, M. (2015). XBeach 1d–Probabilistic Model: ADIS, Settings, Model Uncertainty and Graphical User Interface. *Tec. Rep.* 1209436.

van Rijn, L. C. (2011). Coastal Erosion and Control. *Ocean. Coast. Manage.* 54, 867–887. doi: 10.1016/j.ocecoaman.2011.05.004

Vousdoukas, M. I., Almeida, L. P. M. and Ferreira, Õ. (2012). Beach Erosion and Recovery During Consecutive Storms at a Steep-Sloping, Meso-Tidal Beach. *Earth Surface. Processes. Landforms.* 37, 583–593. doi: 10.1002/esp.2264

Wong, A. (2016). *Wave Hydrodynamics in Ports: Numerical Model Assessment of XBeach*. MSc Thesis, Delft University of Technology (repository.tudelft.nl).

Zhang, K., Douglas, B. C. and Leatherman, S. P. (2004). Global Warming and Coastal Erosion. *Climatic. Change* 64, 41–58. doi: 10.1023/B:CLIM.0000024690.32682.48

Conflict of Interest : Author SH is employed by Sekwang Engineering Consultants Company Limited, and author KK is employed by GeoSystem Research Corporation.The remaining authors declare that the research was conducted in the absence of any commercial or financial relationships that could be construed as a potential conflict of interest.

Publisher's Note: All claims expressed in this article are solely those of the authors and do not necessarily represent those of their affiliated organizations, or those of the publisher, the editors and the reviewers. Any product that may be evaluated in this article, or claim that may be made by its manufacturer, is not guaranteed or endorsed by the publisher.